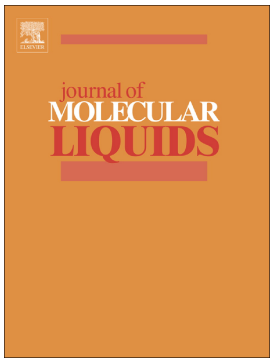

Entropy analysis for comparative study of effective Prandtl number and without effective Prandtl number via γAl2O3-H2O and γAl2O3 -C2H6O2 nanoparticles

T. Hayat, Faisal Shah, M. Ijaz Khan, M. Imran Khan, A. Alsaedi

PII: S0167-7322(18)32161-5
DOI: doi:10.1016/j.molliq.2018.06.029
Reference: MOLLIQ 9227

To appear in: *Journal of Molecular Liquids*

Received date: 24 April 2018
Revised date: 6 June 2018
Accepted date: 7 June 2018

Please cite this article as: T. Hayat, Faisal Shah, M. Ijaz Khan, M. Imran Khan, A. Alsaedi , Entropy analysis for comparative study of effective Prandtl number and without effective Prandtl number via γAl2O3-H2O and γAl2O3 -C2H6O2 nanoparticles. Molliq (2018), doi:10.1016/j.molliq.2018.06.029

Entropy analysis for comparative study of effective Prandtl number and without effective Prandtl number via γAl_2O_3-H_2O and γAl_2O_3-$C_2H_6O_2$ nanoparticles

T. Hayat[a,b], Faisal Shah[a], M. Ijaz Khan[a,1], M. Imran Khan[c,2] and A. Alsaedi[b]

[a]Department of Mathematics, Quaid-I-Azam University 45320 Islamabad 44000, Pakistan

[b]Nonlinear Analysis and Applied Mathematics (NAAM) Research Group, Department of Mathematics, Faculty of Science, King Abdulaziz University, P. O. Box 80257, Jeddah 21589, Saudi Arabia

[c]School of Engineering, University of Portsmouth, Winston Churchill Avenue Portsmouth PO1 2UP, United Kingdom

Abstract: We investigate entropy generation optimization regarding heat source/sink in nonlinear radiative flow over a stretched surface. Thermodynamic second law is invoked in mathematical modeling. Effective Prandtl number model has been used to examine the characteristics of viscous nanomaterial flow with entropy generation. Considered nanoparticles are ($\gamma Al_2O_3 - H_2O$ and $\gamma Al_2O_3 - C_2H_6O_2$). Viscous dissipation and mixed convection are also examined. An optimal homotopy technique leads to solutions development. Optimal values of auxiliary parameters are calculated. Comparison between effective Prandtl number and without effective Prandtl is investigated. Total entropy generation rate is obtained. It is examined from obtained results that velocity is increased by higher estimation of nanoparticle volume fraction. Temperature reduces for higher rate of nanoparticles volume fraction in case of effective Prandtl number while opposite behavior is observed for without effective Prandtl number. Here entropy generation strongly depend upons

[1]Corresponding author

Email address: mikhan@math.qau.edu.pk

[2]Corresponding author

Email address: muhammad.khan4@myport.ac.uk

values of Brinkman number, radiation and temperature ratio parameter. Impacts of radiation and Brinkman number on Bejan number are quite reverse. Main conclusions are presented in concluding remarks.

Keywords: Entropy generation; Effective Prandtl number model; Mixed convection; Viscous dissipation; Nonlinear thermal radiation; Heat source/sink.

1 Introduction

Entropy of thermodynamically framework refers to inaccessibility of valuable work. Entropy generation physically linked with thermodynamical irreversibility and common in all types of heat transport. A higher rate of irreversibility in thermal system dismisses the useful work and decays the proficiency of system. Effectiveness of industrial and mechanical devices can be decreased through existence of irreversibilities. Thermodynamics second law is more reliable and effective than thermodynamics first law. Recently numerous engineers and researchers implemented second law of thermodynamics in thermal manufacturing engineering. Rashidi et al. [1] investigated entropy analysis through second law of thermodynamics for MHD nanomaterial flow by a stretchable porous disk. Entropy generation in vicous fluid flow by stretching sheet is studied by Rashidi et al. [2]. Flow is discussed via effective and without effective Prandtl numbers for both $\gamma Al_2O_2 - H_2O$ and $\gamma Al_2O_2 - C_2H_6O_2$ nanofluids. Hayat et al. [3] discussed entropy generation optimization through second law of thermodynamics via nonlinear radiative heat flux. Flow is examined over a stretched sheet involving Brownian motion and thermophoresis. Later same problem for rotating disk is studied in Hayat et al. [4]. Govindaraju et al. [5] considered magneto-hydrodynamic flow of viscous nanomaterial subject to entropy. Dalir [6] presented forced convective flow of viscoelastic liquid with entropy. Implicit Keller's box technique is implemented for the development

of computational analysis. Sumaira et al. [7] explored dissipative nonlinear radiation and entropy in flow between two rotating disks. Dalir et al. [8] investigated Jeffrey nanomaterial flow with MHD and entropy generation. Sheikholeslami and Ganji [9] scrutinized nanomaterial flow with entropy generation. Lopez et al. [10] examined nonlinear radiative nanofluid flow with convective condition and slip effects. Few recent investigations relevant to this title can be mentioned in Refs. [11 − 25].

Recently, nanotechnology has attracted attention of numerous researchers for its many applications in industrial and mechanical engineering i.e., cancer diagnosis and therapy, drug delivery, photodynamic therapy, non-porous materials for size exclusion chromatography, surgery, neuro electronic interfaces, shedding new light on cells, vivotherapy and molecular motors like kinesis etc. Improvement of heat transport in thermal and mechanical systems are also encountered. Various base liquids like ethylene, oil, water and glycols etc., for viscous and non-Newtonian fluids have minimum thermal conductivity. Therefore such types of liquids have poor heat transport. Thus an increase in thermal performance of such liquids seems quite important for achieving the expectations of researchers and engineers. Choi [26] initially utilized the term nanofluid to enhance the thermal performance of continuous phase liquid. Casson nanoliquid flow due permeable stretchable cylinder with slip is studied by Usman et al. [27]. Sajid et al. [28] explored chemically reactive flow of viscoelastic nanofluid. Sheikholeslami et al. [29] discussed forced convection nanoliquid flow with Lorentz effect towards a stretched sheet. Gireesha et al. [30] examined dusty nanomaterial flow by implementing KVL model. Mair et al. [31] studied nanoliquid flow of Williamson model with inclined Lorentz force effect. Hayat et al. [32] scrutinized nanoliquid flow of second grade fluid in the presence of magnetohydrodynamics. Khan et al. [33] studied couple stress nanoliquid flow with mixed convection and heat source/sink. Latif et al. [34] examined time-

dependent Sisko nanomaterial flow in the presence of variable thermal conductivity and heat source/sink. MHD viscous dissipative flow of micropolar liquid via nonlinear stretchable surface is pointed by Hsiao [35].

This communication develops mathematical model for entropy generation in viscous flow over a stretched surface. Considered flow is discussed for effective and without effective Prandtl numbers. Nonlinear thermal radiation and heat source/sink are accounted. Governing problems are solved by optimal homotopy technique (OHAM) [36 − 45]. Momentum, energy, entropy generation and Bejan number have been analyzed for both ($\gamma Al_2O_3 - H_2O$ and $\gamma Al_2O_3 - C_2H_6O_2$) nanofluids with effective and without effective Prandtl numbers. Velocity and temperature gradients are graphically discussed.

2 Mathematical modeling

Steady two-dimensional flow of incompressible viscous nanomaterial bounded by a stretching sheet is studied. The stretched surface coincides at $y = 0$ (Fig. 1). Nonlinear thermal radiation and heat source/sink in thermal expression are present. Boundary layer formulation for problem under consideration is [2]:

$$\frac{\partial u}{\partial x} + \frac{\partial v}{\partial y} = 0, \tag{1}$$

$$u\frac{\partial u}{\partial x} + v\frac{\partial u}{\partial y} = \frac{\mu_{nf}}{\rho_{nf}}\frac{\partial^2 u}{\partial y^2} + g\frac{(\rho\beta)_{nf}}{\rho_{nf}}(T - T_\infty), \tag{2}$$

$$\left(u\frac{\partial T}{\partial x} + v\frac{\partial T}{\partial y}\right) = \frac{k_{nf}}{(\rho c_p)_{nf}}\frac{\partial^2 T}{\partial y^2} + \frac{1}{(\rho c_p)_{nf}}\left(\frac{\partial q_r}{\partial y}\right) + \frac{\mu_{nf}}{(\rho c_p)_{nf}}\left(\frac{\partial u}{\partial y}\right)^2 + \frac{Q_0}{(\rho c_p)_{nf}}(T - T_\infty), \tag{3}$$

$$\left.\begin{aligned} u = u_w = ax, \quad v = 0, \quad T = T_w \text{ at } y = 0, \\ u \to 0, \quad T \to T_\infty \quad \text{when } y \to \infty. \end{aligned}\right\} \tag{4}$$

In the above expressions u and v indicate velocity components, x, y cartesian coordinates, μ_{nf} dynamic viscosity, ρ_{nf} density, g gravitational acceleration, β_{nf} thermal expansion co-

efficient, T temperature, T_∞ ambient temperature, k_{nf} thermal conductivity, c_p specific heat capacity, q_r thermal radiative heat flux, Q_0 heat generation/absorption coefficient, u_w stretching velocity, a positive constant and T_w surface temperature.

3 Thermophysical characteristics of $Al_2O_3 - H_2O$ and $Al_2O_3 - C_2H_6O_2$ nanoparticles (nanofluids)

The effective thermal expansion coefficient ($(\rho\beta)_{nf}$), dynamic density $\left(\rho_{nf}\right)$ and heat capacitance $(\rho c_p)_{nf}$ of the nanofluid satisfy [2]:

$$\frac{\rho_{nf}}{\rho_f} = (1-\phi) + \rho\frac{\rho_s}{\rho_f}, \tag{5}$$

$$\frac{(\rho c_p)_{nf}}{(\rho c_p)_f} = (1-\phi) + \phi\frac{(\rho c_p)_s}{(\rho c_p)_f}, \tag{6}$$

$$\frac{(\rho\beta)_{nf}}{(\rho\beta)_f} = (1-\phi) + \phi\frac{(\rho\beta)_s}{(\rho\beta)_f}, \tag{7}$$

in the above equations ϕ stands for nanofluid solid volume fraction.

Dynamic viscosity of nanomaterial (nanofluid) is expressed as [2]:

$$\frac{\mu_{nf}}{\mu_f} = 123\phi^2 + 7.3\phi + 1, \text{ for } Al_2O_3 - H_2O, \tag{8}$$

$$\frac{\mu_{nf}}{\mu_f} = 306\phi^2 - 0.19\phi + 1 \text{ for } Al_2O_3 - C_2H_6O_2, \tag{9}$$

Effective thermal conductivity of nanomaterial (nanofluid) is [46,47]:

$$\frac{k_{nf}}{k_f} = 4.97\phi^2 + 2.72\phi + 1 \text{ for } Al_2O_3 - H_2O, \tag{10}$$

$$\frac{k_{nf}}{k_f} = 28.905\phi^2 + 2.8273\phi + 1 \text{ for } Al_2O_3 - C_2H_6O_2, \tag{11}$$

Effective Prandtl number of nanomaterial (nanofluid) is [48,49]:

$$\frac{\mathrm{Pr}_{nf}}{\mathrm{Pr}_{f}} = 82.1\phi^2 + 3.9\phi + 1 \text{ for } \gamma Al_2O_3 - H_2O, \tag{12}$$

$$\frac{\mathrm{Pr}_{nf}}{\mathrm{Pr}_{f}} = 254.3\phi^2 + 3\phi + 1 \text{ for } Al_2O_3 - C_2H_6O_2, \tag{13}$$

Eqs. $(5-7)$ are the general relationship to calculate the specific heat and density for nanoliquids, Eqs. $(8-9)$ described the dynamic viscosity of nanoliquids $[46-47]$, Eqs. $(10-11)$ presents the Crosser and Hamilton model for effective thermal conductivity $[48-49]$, Eqs. $(12-13)$ highlights effective Prandtl number for γAl_2O_3 nanoliquid which are calculated through regression laws [50].

Table 1: Different thermophysical attributes of ethylene glycol ($C_2H_6O_2$), water (H_2O) and alumina (Al_2O_3) [2]:

	$C_p(Jk^{-1}g^{-1}K^{-1})$	$\rho(kgm^{-3})$	$\beta \times 10^{-5}\,(K^{-1})$	$k(Wm^{-1}K^{-1})$
Alumina (Al_2O_3)	765	3970	0.85	40
Water (H_2O)	4182	998.3	20.06	0.60
Ethylene glycol ($C_2H_6O_2$)	2382	1116.6	65	0.249

We consider the transformations

$$\eta = \sqrt{\frac{a}{\upsilon_f}}y,\ u = axf'(\eta),\ v = -\sqrt{a\upsilon_f}f(\eta),\ \theta(\eta) = \frac{T - T_\infty}{(T_w - T_\infty)}. \tag{14}$$

4 Dimensionless form of flow expressions

4.1 Momentum equation

The momentum equations for both ($\gamma Al_2O_3 - H_2O$ and $\gamma Al_2O_3 - C_2H_6O_2$) nanofluids, are

$$\left.\begin{array}{c}(123\phi^2 + 7.3\phi + 1)f''' + \left(1 - \phi + \phi\frac{\rho_s}{\rho_f}\right)(ff'' + f'^2) \\ + \left(1 - \phi + \phi\frac{\rho_s}{\rho_f}\frac{\beta_s}{\beta_f}\right)\lambda\theta(\eta) = 0, \text{ for } \gamma Al_2O_3 - H_2O\end{array}\right\} \tag{15}$$

$$\left.\begin{array}{c}(306\phi^2 - 0.19\phi + 1)f''' + \left(1 - \phi + \phi\frac{\rho_s}{\rho_f}\right)(ff'' + f'^2) \\ + \left(1 - \phi + \phi\frac{\rho_s}{\rho_f}\frac{\beta_s}{\beta_f}\right)\lambda\theta(\eta) = 0, \text{ for } \gamma Al_2O_3 - C_2H_6O_2\end{array}\right\} \tag{16}$$

$$f(0) = 0,\ f'(0) = 1,\ f'(\infty) = 0, \tag{17}$$

in which $\lambda\left(= \frac{g\beta_f b}{a^2}\right)$ denotes the mixed convection parameter.

4.2 Energy equation

In dimensionless form the energy equations for both ($\gamma Al_2O_3 - H_2O$ and $\gamma Al_2O_3 - C_2H_6O_2$) nanofluids are

$$\left.\begin{array}{c}\frac{d}{d\eta}\left[(4.97\phi^2 + 2.72\phi + 1) + R_d(1 + (\theta_w - 1)\theta)^3\theta'(\eta)\right] \\ +\Psi\left[\begin{array}{c} f(\eta)\theta'(\eta) - f'(\eta)\theta(\eta) + \frac{Ec}{\left(1-\phi+\phi\frac{(\rho c_p)_s}{(\rho c_p)_f}\right)}(f''(\eta))^2 \\ +\frac{\gamma}{\left(1-\phi+\phi\frac{(\rho c_p)_s}{(\rho c_p)_f}\right)}\theta(\eta)\end{array}\right] = 0, \text{for } \gamma Al_2O_3 - H_2O\end{array}\right\} \tag{18}$$

$$\left.\begin{array}{c}\frac{d}{d\eta}\left[(28.905\phi^2 + 2.8273\phi + 1) + R_d(1 + (\theta_w - 1)\theta)^3\theta'(\eta)\right] \\ +\Psi\left[\begin{array}{c} f(\eta)\theta'(\eta) - f'(\eta)\theta(\eta) + \frac{Ec}{\left(1-\phi+\phi\frac{(\rho c_p)_s}{(\rho c_p)_f}\right)}(f''(\eta))^2 \\ +\frac{\gamma}{\left(1-\phi+\phi\frac{(\rho c_p)_s}{(\rho c_p)_f}\right)}\theta(\eta)\end{array}\right] = 0, \text{for } \gamma Al_2O_3 - C_2H_6O_2\end{array}\right\} \tag{19}$$

$$\theta(0) = 1 \quad \theta(\infty) = 0, \tag{20}$$

where Ψ depicts effective Prandtl number via $\gamma Al_2O_3 - H_2O$ and $\gamma Al_2O_3 - C_2H_6O_2$ nanofluids which in mathematical form is defined by [2]:

$$\Psi = \frac{(\mathrm{Pr})_f \left(1 - \phi + \phi \frac{\rho_s}{\rho_f}\right) (82.1\phi^2 + 3.9\phi + 1)}{123\phi^2 + 7.3\phi + 1}, \tag{21}$$

$$\Psi = \frac{(\mathrm{Pr})_f \left(1 - \phi + \phi \frac{\rho_s}{\rho_f}\right) (254.3\phi^2 - 3\phi + 1)}{306\phi^2 - 0.19\phi + 1}, \tag{22}$$

In absence of effective Prandtl number via $\gamma Al_2O_3 - H_2O$ and $\gamma Al_2O_3 - C_2H_6O_2$ nanofluids one has [2]:

$$\Psi = \frac{(\mathrm{Pr})_f \left(1 - \phi + \phi \frac{\rho_s}{\rho_f}\right)}{4.97\phi^2 - 2.72\phi + 1}, \tag{23}$$

$$\Psi = \frac{(\mathrm{Pr})_f \left(1 - \phi + \phi \frac{\rho_s}{\rho_f}\right)}{28.905\phi^2 + 2.8273\phi + 1}, \tag{24}$$

where $R_d \left(= \frac{16\sigma^* T_\infty^3}{3kk_f}\right)$ represents the radiation parameter, $Ec \left(= \frac{u_w^2}{ac_p}\right)$ the Eckert number and $\gamma \left(= \frac{Q_o}{\rho c_p}\right)$ the heat source/sink parameter.

5 Physically quantities of interests

5.1 Coefficient of skin friction

we have

$$C_f = \frac{\tau_w}{\rho_f u_w^2}, \tag{25}$$

where shear stress τ_w is defined as

$$\tau_w = -2\mu_{nf}\big|_{y=0} \left.\frac{\partial u}{\partial y}\right|_{y=0}, \tag{26}$$

The above expressions yield

$$\left.\begin{aligned} \tfrac{1}{2}\sqrt{\mathrm{Re}_x}C_f &= -\left(123\varphi^2 + 7.3\varphi + 1\right) f''(0) \text{ for } \gamma Al_2O_3 - H_2O, \\ \tfrac{1}{2}\sqrt{\mathrm{Re}_x}C_f &= -\left(306\varphi^2 - 0.19\varphi + 1\right) f''(0) \text{ for } \gamma Al_2O_3 - C_2H_6O_2. \end{aligned}\right\} \tag{27}$$

5.2 Nusselt number (Heat transfer rate)

Mathematically we have

$$Nu = \frac{xq_w}{k_f\left(T_w - T_\infty\right)}, \tag{28}$$

where wall flux q_w is expressed as

$$q_w = -k_{nf}\left(1 + \frac{16\sigma T^3}{3kk_f}\right)\left(\frac{\partial T}{\partial y}\right)_{y=0}. \tag{29}$$

Invoking Eq. (29) in Eq. (28) we have

$$\left.\begin{aligned} (\mathrm{Re}_x)^{-1/2}Nu_x &= \left[\begin{array}{c} (4.97\varphi^2 + 2.72\varphi + 1) \\ +R_d(1 + (\theta_w - 1)\theta(0))^3\theta'(0) \end{array}\right] \text{ for } \gamma Al_2O_3 - H_2O, \\ (\mathrm{Re}_x)^{-1/2}Nu_x &= \left[\begin{array}{c} (28.905\varphi^2 + 2.8273\varphi + 1) \\ +R_d(1 + (\theta_w - 1)\theta(0))^3\theta'(0) \end{array}\right] \text{ for } \gamma Al_2O_3 - C_2H_6O_2, \end{aligned}\right\} \tag{30}$$

in which $\mathrm{Re}_x\left(=\frac{xu_w}{\nu_f}\right)$ indicates the local Reynolds number.

6 Mathematical modeling of entropy generation

For this model volumetric entropy generation can be written as

$$S_g = \frac{k_f}{T_\infty^2}\left[\frac{k_{nf}}{k_f}\left(\frac{\partial T}{\partial y}\right)^2 + \frac{16\sigma^* T_\infty^3}{3kk_f}\left(\frac{\partial T}{\partial y}\right)^2\right] + \frac{\mu_{nf}}{T_\infty}\left(\frac{\partial u}{\partial y}\right)^2, \tag{31}$$

The characteristic entropy generation rate is expressed as

$$(S_g)_0 = \frac{k_{nf}}{T_\infty^2}\frac{(\Delta T)^2}{x^2}, \tag{32}$$

Mathematically total entropy generation is the combination (ratio) of volumetric entropy rate and characteristic entropy rate i.e.,

$$S_G = \frac{S_g}{(S_g)_0}. \tag{33}$$

The dimensionless form of above equations for both ($\gamma Al_2O_3 - H_2O$ and $\gamma Al_2O_3 - C_2H_6O_2$) nanofluids are

$$\left.\begin{aligned} S_G = \theta^2(\eta) + \mathrm{Re}\left[(4.97\phi^2 + 2.72\phi + 1) + R_d(1 + (\theta_w - 1)\theta(0))^3\theta'^2(0)\right] \\ + \left[\tfrac{123\phi^2+7.3\phi+1}{4.97\phi^2+2.72\phi+1}\right]\tfrac{Br}{\Omega}\,\mathrm{Re}\, f''^2, \text{ for } \gamma Al_2O_3 - H_2O \end{aligned}\right\} \tag{34}$$

$$\left.\begin{aligned} S_G = \theta^2(\eta) + \mathrm{Re}\left[(28.905\phi^2 + 2.8273\phi + 1) + R_d(1 + (\theta_w - 1)\theta(0))^3\theta'^2(0)\right] \\ + \left[\tfrac{306\phi^2-0.19\phi+1}{28.905\phi^2+2.8273\phi+1}\right]\tfrac{Br}{\Omega}\,\mathrm{Re}\, f''^2, \text{ for } \gamma Al_2O_3 - C_2H_6O_2 \end{aligned}\right\} \tag{35}$$

Dimensionless forms of Bejan number are defined by

$$\left.\begin{aligned} Be = \frac{\mathrm{Re}\left[(4.97\phi^2 + 2.72\phi + 1) + R_d(1 + (\theta_w - 1)\theta(0))^3\theta'^2(0)\right]}{\theta^2(\eta) + \mathrm{Re}\left[\begin{array}{c}(4.97\phi^2 + 2.72\phi + 1)\\ +R_d(1 + (\theta_w - 1)\theta(0))^3\theta'^2(0)\end{array}\right] + \left[\tfrac{123\phi^2+7.3\phi+1}{4.97\phi^2+2.72\phi+1}\right]\tfrac{Br}{\Omega}\,\mathrm{Re}\, f''^2}, \text{ for } \gamma Al_2O_3 - H_2O \end{aligned}\right\} \tag{36}$$

$$\left.\begin{aligned} Be = \frac{\mathrm{Re}\left[(28.905\phi^2 + 2.8273\phi + 1) + R_d(1 + (\theta_w - 1)\theta(0))^3\theta'^2(0)\right]}{\theta^2(\eta) + \mathrm{Re}\left[\begin{array}{c}(28.905\phi^2 + 2.8273\phi + 1)\\ +R_d(1 + (\theta_w - 1)\theta(0))^3\theta'^2(0)\end{array}\right] + \left[\tfrac{306\phi^2-0.19\phi+1}{28.905\phi^2+2.8273\phi+1}\right]\tfrac{Br}{\Omega}\,\mathrm{Re}\, f''^2}, \gamma Al_2O_3 - C_2H_6O_2 \end{aligned}\right\} \tag{37}$$

in which $Br\left(=\frac{\mu_f}{k_f\Delta T}\right)$ denotes the Brinkman number and $\Omega\left(=\frac{\Delta T}{T_\infty}\right)$ the temperature difference parameter.

7 Solutions by OHAM

Initial approximations $(f_0(\eta),\ \theta_0(\eta))$ and linear operators $(\mathcal{L}_f(f), \mathcal{L}_\theta(\theta))$ have been chosen as

$$\left.\begin{aligned} f_0(\eta) = 1-\exp(-\eta),\ \theta_0(\eta) = \exp(-\eta), \\ \mathcal{L}_f(f) = \tfrac{d^3f}{d\eta^3} - \tfrac{df}{d\eta},\ \mathcal{L}_\theta(\theta) = \tfrac{d^2\theta}{d\eta^2} - \theta, \end{aligned}\right\} \tag{38}$$

with

$$\left.\begin{aligned} \mathcal{L}_f\left[D_1^* + D_2^*\exp(\eta) + D_3^*\exp(-\eta)\right] = 0, \\ \mathcal{L}_\theta\left[D_4^*\exp(\eta) + D_5^*\exp(-\eta)\right] = 0, \end{aligned}\right\} \tag{39}$$

where D_i^* $(i = 1-5)$ highlights the arbitrary constants.

The mathematical formula for average squared residual error of velocity and temperature equations at k^{th} order are

$$\varepsilon_m^f(h_f) = \frac{1}{N+1}\sum_{j=0}^{N}\left[\sum_{i=0}^{m}(f_i)_{\eta=j\Pi\eta}\right]^2, \tag{40}$$

$$\varepsilon_m^\theta(h_f,h_\theta) = \frac{1}{N+1}\sum_{j=0}^{N}\left[\sum_{i=0}^{m}(f_i)_{\zeta=j\Pi\eta}, \sum_{i=0}^{m}(\theta_i)_{\eta=j\Pi\eta}\right]^2. \tag{41}$$

The total error is defined as follows:

$$\varepsilon_m^t = \varepsilon_m^f + \varepsilon_m^\theta, \tag{42}$$

in which ε_m^t stands for total square residual error. Optimal values of convergence control parameters ($R_d = 0.4$, $\theta_w = 1.1$, $Br = 0.4$, $\gamma = 0.1$, Re $= 0.3$, $\lambda = 0.2$, Pr $= 1.0$ and $Ec = 0.1$) are $h_f = -0.85698$ and $h_\theta = -0.312346$. The numerical values of total residual error is $\varepsilon_m^t = 9.20133\times10^{-6}$.

Table 2: Individual residual errors for different flow variables when $R_d = 0.4$, $\theta_w = 1.1$, $Br = 0.4$, $\gamma = 0.1$, Re $= 0.3$, $\lambda = 0.2$, Pr $= 1.0$ and $Ec = 0.1$.

m	ε_m^f	ε_m^θ
2	8.94180×10^{-8}	6.84831×10^{-6}
6	5.20171×10^{-12}	6.1285×10^{-8}
8	3.21087×10^{13}	5.15682×10^{-8}
10	3.58381×10^{-15}	508389×10^{-10}
16	1.2359×10^{-21}	2.58971×10^{-11}
22	2.5872×10^{-24}	3.80485×10^{-12}
24	1.58101×10^{-27}	5.9729×10^{-14}

8 Outcomes and analysis

In this section, the computations are carried out for various flow parameters like Prandtl number (Pr), mixed convection parameter (λ), heat source parameter (γ), nanoparticles volume fraction (ϕ), radiation parameter (R_d), temperature ratio parameter (θ_w), Eckert number (Ec) and Brinkman number (Br). To get a definite interpretation of derived flow expressions, the velocity, temperature and entropy generation are plotted graphically in Figs. $2-12$ by implementing optimal homotopy method (OHAM). Table 1 highlights themophysical attributes of ethylene glycol ($C_2H_6O_2$), water (H_2O) and alumina (Al_2O_3). Table 2 represents the average residual error for momentum and temperature equations via different estimations of auxiliary parameters.

Impact of nanoparticles volume fraction on velocity is sketched in Figs. $2(a, b)$. From Figs. $2(a, b)$ it is examined that (ϕ) significantly enhances the velocity ($f'(\eta)$) for both $\gamma Al_2O_3 - H_2O$ and $\gamma Al_2O_3 - C_2H_6O_2$ nanofluids. Behavior of nanoparticle volume frac-

tion on thermal field is shown in Figs. $3(a,b)$. In Fig. $3(a)$ the temperature has contrasting situation for effective Prandtl number and without effective Prandtl number in $\gamma Al_2O_3 - H_2O$ nanofluid. For positive estimations of nanoparticles volume fraction ($\phi = 0.00, 0.01, 0.02, 0.03, 0.04$) temperature field decays in case of effective Prandtl number while an enhancement is examined for larger nanoparticles volume fraction in without effective Prandtl number situation. Similar results is observed for rising estimations of nanoparticles volume fraction for both effective Prandtl number and without effective Prandtl number in $\gamma Al_2O_3 - C_2H_6O_2$ nanofluids (see Fig. $3b$). Figs. $4(a)$ and $4(b)$ disclose the behavior of temperature field via positives values of Eckert number ($Ec = 1.0, 2.0, 3.0, 4.0$). From Fig. $4(a)$ temperature is more about increasing values of Eckert number both effective and without effective Prandtl numbers for case of $\gamma Al_2O_3 - H_2O$. Physically higher estimations of Eckert number show a rapid change in thermal field due to fractional heating for both cases $\gamma Al_2O_3 - H_2O$ and $\gamma Al_2O_3 - C_2H_6O_2$ (see Figs. $4(a,b)$. Eckert number (Ec) represents quantitative relationship between enthalpy and kinetic energy. For higher estimation of Eckert number means that thermal dissipated heat is stored in the liquid which upsurge the temperature field. Figs. $5(a,b)$ display the impact of (R_d) on temperature. We examined an enhancement in temperature field via larger radiative parameter for both effective and without effective Prandtl numbers. Physically radiative parameter enhances the surface heat flux which is responsible for an increment in thermal field for both effective and without effective Prandtl numbers in $\gamma Al_2O_3 - H_2O$ and $\gamma Al_2O_3 - C_2H_6O_2$ nanofluids.

Variation of Brinkman number on entropy generation ($S_G(\eta)$) is shown in Figs. $6(a,b)$. Here entropy generation via Brinkman number enhances for both $\gamma Al_2O_3 - H_2O$ and $\gamma Al_2O_3 - C_2H_6O_2$ nanofluids with effective and without effective Prandtl numbers. Physically larger amount of heat is released between layer of liquid particles and consequently

an enhancement is observed in entropy. Figs. $7(a,b)$ illustrate impact of radiation (R_d) on $(S_G(\eta))$ for with and without effective Prandtl numbers in both $\gamma Al_2O_3 - H_2O$ and $\gamma Al_2O_3 - C_2H_6O_2$ nanofluids. From Figs. $7(a,b)$, it is examined that for an enhancement in radiation there is remarkable increase in $(S_G(\eta))$. It is also observed that entropy dominantes in case of without effective Prandtl number when compared with effective Prandtl number for cases of $\gamma Al_2O_3 - H_2O$ and $\gamma Al_2O_3 - C_2H_6O_2$. Consequences of temperature ratio variable on $(S_G(\eta))$ are shown in Figs. $8(a,b)$. Here $(S_G(\eta))$ enhanced via temperature ratio variable for both $\gamma Al_2O_3 - H_2O$ and $\gamma Al_2O_3 - C_2H_6O_2$ nanofluids and with and without effective Prandtl numbers. Physically for higher estimations of temperature difference variable the irreversibility rate of system increases and so $(S_G(\eta))$ enhances. Furtherrmore it is also found that $(S_G(\eta))$ dominantes in case of effective Prandtl number when compared for without effective Prandtl number in the presence of $\gamma Al_2O_3 - H_2O$ and $\gamma Al_2O_3 - C_2H_6O_2$ nanofluids.

Characteristics of (Br) on Bejan number (Be) is displayed in Figs. $9(a,b)$. From Figs. $(9(a,b))$, it is analyzed that (Be) is decreasing function of (Br) for both $\gamma Al_2O_3 - H_2O$ and $\gamma Al_2O_3 - C_2H_6O_2$ nanofluids and with and without effective Prandtl numbers. In fact viscous effect dominantes for larger (Br) and so Bejan number decays. Salient features of radiation (R_d) on (Be) is explored in Figs. $10(a,b)$. Bejan number enhances when (R_d) increases for both $\gamma Al_2O_3 - H_2O$ and $\gamma Al_2O_3 - C_2H_6O_2$ nanofluids and cases of effective and without effective Prandtl numbers. Physically internal energy of system increases and as a result Bejan number enhances.

Figs. $11(a,b)$ highlight the behavior of skin friction coefficient through mixed convection parameter (λ) and (ϕ). Magnitude of skin friction increases via larger nanoparticles volume fraction and mixed convection in both $\gamma Al_2O_3 - H_2O$ and $\gamma Al_2O_3 - C_2H_6O_2$ nanofluids and

with and without effective Prandtl numbers (see Figs. $11(a,b)$). Nusselt number through Eckert number and nanoparticles volume fraction for both $\gamma Al_2O_3 - H_2O$ and $\gamma Al_2O_3 - C_2H_6O_2$ nanofluids are sketched in Figs. $12(a,b)$. Heat transfer rate is increased with (ϕ) and Eckert number for both effective and without effective Prandtl numbers. Furthermore heat transfer dominantes in case of effective Prandtl number when compared to without effective Prandtl number.

9 Conclusions

Here viscous fluid flow with $\gamma Al_2O_3 - H_2O$ and $\gamma Al_2O_3 - C_2H_6O_2$ nanomaterials for effective and without effective Prandtl numbers is studied. Main conclusions of study are listed below:

- Velocity field in the presence of $\gamma Al_2O_3 - H_2O$ and $\gamma Al_2O_3 - C_2H_6O_2$ nanofluids increases for higher nanoparticles volume fraction.
- Temperature has dual behavior for with and without effective Prandtl numbers.
- $(S_G(\eta))$ is increased for higher Br, R_d and θ_w.
- Influences of (Br) and (R_d) on Bejan number are quite reverse.
- Mixed convection leads to an enhancement in magnitude of skin friction coefficient and heat transfer rate.

10 Compliance with ethical standards

10.1 Sources of financial funding and support

There are no funders to report for this submission.

10.2 Conflict of interest

The authors declare that they have no conflict of interest.

References

[1] M.M. Rashidi, S. Abelman and N. Freidoonimehr, Entropy generation in steady MHD flow due to a rotating porous disk in a nanofluid, International Journal of Heat and Mass Transfer 62 (2013) 515-525.

[2] M. M. Rashidi, N. Vi. Ganesh, A. K. A. Hakeem, B. Ganga and G. Lorenzini, Influences of an effective Prandtl number model on nano boundary layer flow of $\gamma Al_2O_3 - H_2O$ and $\gamma Al_2O_3 - C_2H_6O_2$ over a vertical stretching sheet, International Journal of Heat and Mass transfer, 98 (2016) 616-623.

[3] T. Hayat, M. I. Khan, S. Qayyum, A. Alsaedi and M. I. Khan, New thermodynamics of entropy generation minimization with nonlinear thermal radiation and nanomaterials, Physics Letter A, 382 (2018) 749-760.

[4] T. Hayat, M. I. Khan, S. Qayyum and A. Alsaedi, Entropy generation in flow with silver and copper nanoparticles, Colloids and Surfaces A: Physicochemical and Engineering Aspects, 539 (2018) 335-346.

[5] M. Govindaraju, N. V. Ganesh, B. Ganga and A. K. A. Hakeem, Entropy generation analysis of magneto hydrodynamic flow of a nanofluid over a stretching sheet, Journal of the Egyptian Mathematical Society, 23 (2015) 429-434.

[6] N. Dalir, Numerical study of entropy generation for forced convection flow and heat transfer of a Jeffrey fluid over a stretching sheet, Alexandria Engineering Journal, 53 (2014) 769-778.

[7] S. Qayyum, T. Hayat, M. I. Khan, M. I. Khan and A. Alsaedi, Optimization of entropy generation and dissipative nonlinear radiative Von Karman's swirling flow with Soret and Dufour effects, Journal of Molecular Liquids, (2018) In press.

[8] N. Dalir, M. Dehsara and S. S. Nourazar, Entropy analysis for magnetohydrodynamic flow and heat transfer of a Jeffrey nanofluid over a stretching sheet, Energy, 79 (2015) 351-362.

[9] M. Sheikholeslami and D. D. Ganji, Entropy generation of nanofluid by means of semi analytical methods, Applications of semi analytical methods for nanofluid flow and heat transfer, 11 (2018) 511-554.

[10] A. López, G. Ibáñez, J. Pantoja, J. Moreira and O. Lastres, Entropy generation analysis of MHD nanofluid flow in a porous vertical microchannel with nonlinear thermal radiation, slip flow and convective-radiative boundary conditions, International Journal of Heat and Mass Transfer, 107 (2017) 982-994.

[11] Y. S. Daniel, Z. A. Aziz, Z. Ismail and F. Salah, Numerical study of entropy analysis for electrical unsteady natural magnetohydrodynamic flow of nanofluid and heat transfer, Chinese Journal of Physics, 55 (2017) 1821-1848.

[12] M. I. Khan, S. Qayyum, T. Hayat, A. Alsaedi and M. I. Khan, Investigation of Sisko fluid through entropy generation, Journal of Molecular Liquids, 25 (2018) 155-163.

[13] T. Hayat, M. W. A. Khan, M. I. Khan and A. Alsaedi, Nonlinear radiative heat flux and heat source/sink on entropy generation minimization rate, Physica B: Condensed Matter, 538 (2018) 95-103.

[14] N. Freidoonimehr and A. B. Rahimi, Exact-solution of entropy generation for MHD nanofluid flow induced by a stretching/shrinking sheet with transpiration: Dual solution, Advanced Powder Technology, 28 (2017) 671-685.

[15] S. U. Rehman, R. U. Haq, Z. H. Khan and C. Lee, Entropy generation analysis for non-Newtonian nanofluid with zero normal flux of nanoparticles at the stretching surface, Journal of the Taiwan Institute of Chemical Engineers, 63 (2016) 226-235.

[16] M. I. Khan, S. Ullah, T. Hayat, M. Waqas, M. I. Khan and A. Alsaedi, Salient aspects of entropy generation optimization in mixed convection nanomaterial flow, International Journal of Heat and Mass Transfer, (In press).

[17] M. I. Khan, S. Qayyum, T. Hayat, M. I. Khan, A. Alsaedi and T. A. Khan, Entropy generation in radiative motion of tangent hyperbolic nanofluid in presence of activation energy and nonlinear mixed convection, Physics Letter A, 382 (2018) 2017-2026.

[18] M. I. Khan, S. Sumaira, T. Hayat, M. Waqas, M. I. Khan and A. Alsaedi, Entropy generation minimization and binary chemical reaction with Arrhenius activation energy in MHD radiative flow of nanomaterial, Journal of Molecular Liquids, 259 (2018) 274-283.

[19] M. W. A. Khan, M. I. Khan, T. Hayat and A. Alsaedi, Entropy generation minimization (EGM) of nanofluid flow by a thin moving needle with nonlinear thermal radiation, Physica B: Condensed Matter, 534 (2018) 113-119.

[20] M. I. Khan, T. Hayat and A. Alsaedi, Numerical investigation for entropy generation in hydromagnetic flow of fluid with variable properties and slip, AIP, Physics of Fluid, 30 (2018) 023601.

[21] T. Hayat, S. Qayyum, M. I. Khan and A. Alsaedi, Entropy generation in magnetohydrodynamic radiative flow due to rotating disk in presence of viscous dissipation and Joule heating, AIP, Physics of Fluids 30 (2018) 017101.

[22] M. I. Khan, T. Hayat, M. I. Khan and A. Alsaedi, Activation energy impact in nonlinear radiative stagnation point flow of Cross nanofluid, International Communications in Heat and Mass Transfer, 91 (2018) 216-224.

[23] T. Hayat, M.I. Khan, S. Qayyum, M. I. Khan and A. Alsaedi, Entropy generation for flow of Sisko fluid due to rotating disk, Journal of Molecular Liquids, 264 (2018) 375-385.

[24] M. I. Khan, S. Qayyum, T. Hayat, A. Alsaedi and M. I. Khan, Corrigendum to "Investigation of Sisko fluid through entropy generation"[J. Mol. Liq.: In Press (2018), doi. org/10.1016/j. molliq. 2018.02. 087], Journal of Molecular Liquids, 259 (2018) 238.

[25] M. I. Khan, T. A. Khan, S. Qayyum, T. Hayat, M. I. Khan and A. Alsaedi, Entropy generation optimization and activation energy in nonlinear mixed convection flow of tangent hyperbolic nanofluid, The European Physical Journal Plus

[26] S. U. S. Choi, Enhancing thermal conductivity of fluids with nanoparticles, ASME, FED 231/MD 66 (1995) 99-105.

[27] M. Usman, F. A. Soomro, R. U. Haq, W. Wang and O. Defterli, Thermal and velocity slip effects on Casson nanofluid flow over an inclined permeable stretching cylinder

via collocation method, International Journal of Heat and Mass Transfer, 122 (2018) 1255-1263.

[28] S. Qayyum, T. Hayat, A. Alsaedi and B. Ahmad, Magnetohydrodynamic (MHD) nonlinear convective flow of Jeffrey nanofluid over a nonlinear stretching surface with variable thickness and chemical reaction, International Journal of Mechanical Sciences, 134 (2017) 306-314.

[29] M. Sheikholeslami, M. T. Mustafa and D. D. Ganji, Effect of Lorentz forces on forced-convection nanofluid flow over a stretched surface, Particuology, 26 (2016) 108-113.

[30] B. J. Gireesha, B. Mahanthesh, G. T. Thammanna and P. B. Sampathkumar, Hall effects on dusty nanofluid two-phase transient flow past a stretching sheet using KVL model, Journal of Molecular Liquids, 256 (2018) 139-147.

[31] M. Khan, M. Y. Malik, T. Salahuddin and A. Hussian, Heat and mass transfer of Williamson nanofluid flow yield by an inclined Lorentz force over a nonlinear stretching sheet, Results in Physics, 8 (2018) 862-868.

[32] T. Hayat, A. Aziz, T. Muhammad, A. Alsaedi and M. Mustafa, On magnetohydrodynamic flow of second grade nanofluid over a convectively heated nonlinear stretching surface, Advanced Powder Technology, 27 (2016) 1992-2004.

[33] S. U. Khan, S. A. Shehzad, A. Rauf and N. Ali, Mixed convection flow of couple stress nanofluid over oscillatory stretching sheet with heat absorption/generation effects, Results in Physics, 8 (2018) 1223-1231.

[34] M. Khan, L. Ahmad and M. M. Gulzar, Unsteady Sisko magneto-nanofluid flow with heat absorption and temperature dependent thermal conductivity: A 3D numerical study, Results in Physics, 8 (2018) 1092-1103.

[35] K. L. Hsiao, Micropolar nanofluid flow with MHD and viscous dissipation effects towards a stretching sheet with multimedia feature, International Journal of Heat and Mass Transfer, 112 (2017) 983-990.

[36] S. J. Liao, Homotopy Analysis Method in Non-Linear Differential Equations Springer and Higher Education Press, Heidelberg (2012).

[37] T. Hayat, M. I. Khan, M. Farooq, A. Alsaedi, M. Waqas and T. Yasmeen, Impact of Cattaneo-Christov heat flux model in flow of variable thermal conductivity fluid over a variable thicked surface, International Journal of Heat and Mass Transfer, 99 (2016) 702-710.

[38] T. Hayat, M. I. Khan, M. Farooq, T. Yasmeen and A. Alsaedi, Stagnation point flow with Cattaneo-Christov heat flux and homogeneous-heterogeneous reactions, Journal of Molecular Liquids, 220 (2016) 49-55.

[39] Z. Abbas, M. Naveed and M. Sajid, Hydromagnetic slip flow of nanofluid over a curved stretching surface with heat generation and thermal radiation, Journal of Molecular Liquids, 215 (2016) 756-762.

[40] M. Khan, M. Irfan and W. A. Khan, Impact of heat source/sink on radiative heat transfer to Maxwell nanofluid subject to revised mass flux condition, Results in Physics, 9 (2018) 851-857.

[41] M. F. Javed, M. I.Khan, N. B. Khan, R. Muhammad, M. U. Rehmand, S. W. Khan and T. A. Khan, Axisymmetric flow of Casson fluid by a swirling cylinder, Results Phys. 9 (2018), pp. 1250-1255.

[42] N. B. Khan , Z. Ibrahim, L. T. T. Nguyen , M. F. Javed and M. Jameel, Numerical investigation of the vortex-induced vibration of an elastically mounted circular cylinder at high Reynolds number (Re = 10^4) and low mass ratio using the RANS code, Plos One., 12 (2017), pp. e0185832.

[43] N. B. Khan, Z. Ibrahim, M. I. Khan, T. Hayat and M. F.Javed, VIV study of an elastically mounted cylinder having low mass-damping ratio using RANS model, Int. J. Heat Mass Transf., 121 (2018), pp. 309-314.

[44] N. B. Khan, Z. Ibrahim, A. B. B. M. Badry, M. Jameel, M. F. Javed, Numerical investigation of flow around cylinder at Reynolds number = 3900 with large eddy simulation technique: Effect of spanwise length and mesh resolution, Proceedings of the Institution of Mechanical Engineers, Part M: Journal of Engineering for the Maritime Environment, (2018) https://doi.org/10.1177/1475090217751326.

[45] N. B. Khan and Z. Ibrahim, Numerical investigation of vortex-induced vibration of an elastically mounted circular cylinder with One-degree of freedom at high Reynolds number using different turbulent models, Proceedings of the Institution of Mechanical Engineers, Part M: Journal of Engineering for the Maritime Environment, (2018) doi: 10.1177/1475090217751992.

[46] Lee, S., Choi, S.U.-S., Li, S.and Eastman, J.A. Measuring thermal conductivity of fluids containing oxide nanoparticles. Journal of Heat transfer, 121, 280-289 (1999).

[47] X. Wang, X. Xu and S. U. S. Choi, Thermal conductivity of nanoparticles-fluid mixture.Journal of Thermophysics and Heat Transfer, 13, 474-480 (1999).

[48] R. L. Hamilton and O. K. Crosser, Thermal conductivity of heterogeneous two component systems. Industrial & Engineering Chemistry Fundamentals, 1, 187-191 (1962).

[49] S. E. B. Maiga, C. T. Nguyen, N. Galanis and G. Roy, Heat transfer behaviors of nanofluids in a uniformly heated tube. Superlattices and Microstructures, 35, 543-557 (2004).

[50] C. V. Pop, S. Fohanno, G. Polidori and C. T. Nguyen, Analysis of laminar-to-turbulent threshold with water-γAl_2O_3 and ethylene glycol-γAl_2O_3 nanofluids in free convection. In Proceedings of the 5th IASME/WSEAS International Conference on Heat Transfer, Thermal Engineering and Environment, Athens, Greece, 188, $25-27(2017)$.

Figure Captions

Fig. 1: Flow diagram.

Fig.2(a) : ϕ on f' for $\gamma Al_2O_3 - H_2O$.

Fig.2(b) : ϕ on f' for $\gamma Al_2O_3 - C_2H_6O_2$.

Fig.3(a) : ϕ on θ for $\gamma Al_2O_3 - H_2O$.

Fig.3(b) : ϕ on θ for $\gamma Al_2O_3 - C_2H_6O_2$.

Fig.4(a) : Ec on θ for $\gamma Al_2O_3 - H_2O$.

Fig.4(b) : Ec on θ for $\gamma Al_2O_3 - C_2H_6O_2$.

Fig.5(a) : R_d on θ for $\gamma Al_2O_3 - H_2O$.

Fig.5(b) : R_d on θ for $\gamma Al_2O_3 - C_2H_6O_2$.

Fig.6(a) : Br on S_G for $\gamma Al_2O_3 - H_2\dot{O}$.

Fig.6(b) : Br on S_G for $\gamma Al_2O_3 - C_2H_6\dot{O}_2$.

Fig.7(a) : R_d on S_G for $\gamma Al_2O_3 - H_2\dot{O}$.

Fig.7(b) : R_d on S_G for $\gamma Al_2O_3 - C_2H_6\dot{O}_2$.

Fig.8(a) : θ_w on S_G for $\gamma Al_2O_3 - H_2\dot{O}$.

Fig.8(b) : θ_w on S_G for $\gamma Al_2O_3 - C_2H_6\dot{O}_2$.

Fig.9(a) : Br on Be for $\gamma Al_2O_3 - H_2\dot{O}$.

Fig.9(b) : Br on Be for $\gamma Al_2O_3 - C_2H_6\dot{O}_2$.

Fig.10(a) : R_d on Be for $\gamma Al_2O_3 - H_2\dot{O}$.

Fig.10(b) : R_d on Be for $\gamma Al_2O_3 - C_2H_6\dot{O}_2$.

Fig.11(a) : λ and ϕ on C_f for alumina water.

Fig.11(b) : λ and ϕ on C_f for ethylenecglycol .

Fig.12(a) : Ec and ϕ on Nu for alumina water.

Fig.12(b) : Ec and ϕ on Nu for ethylenecglycol .

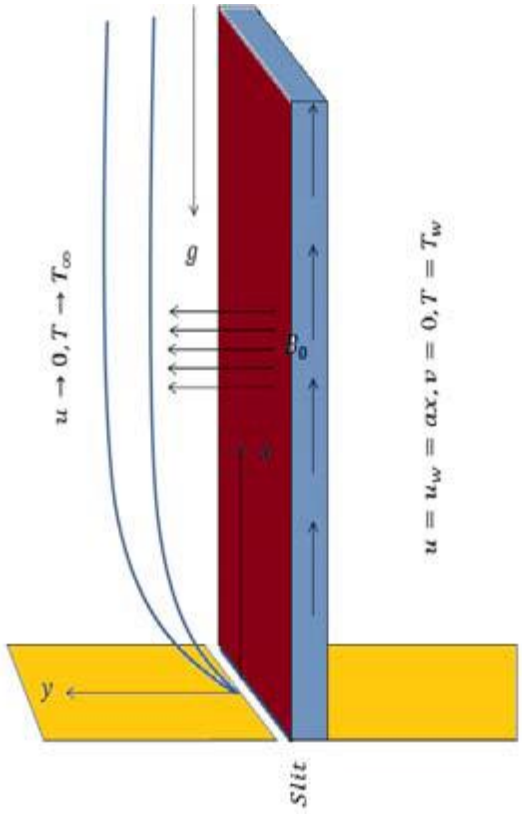

Figure 1

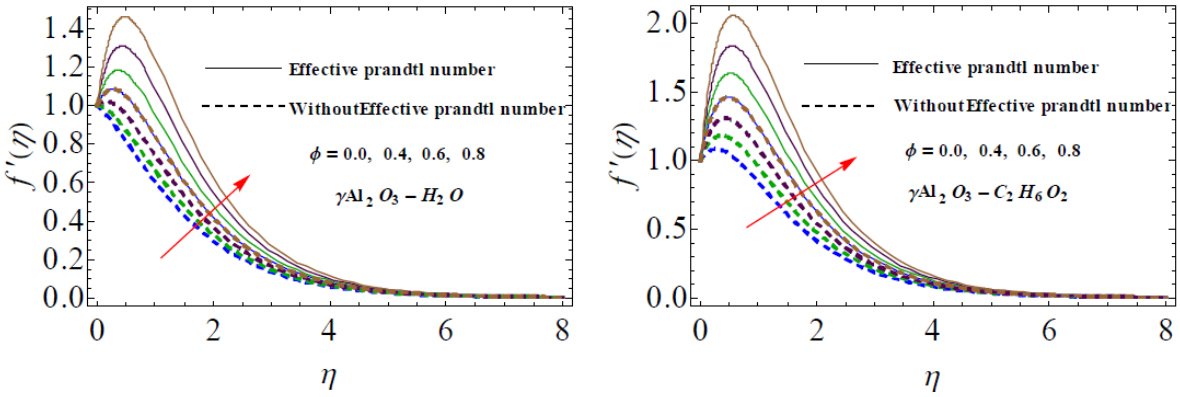

Figure 2

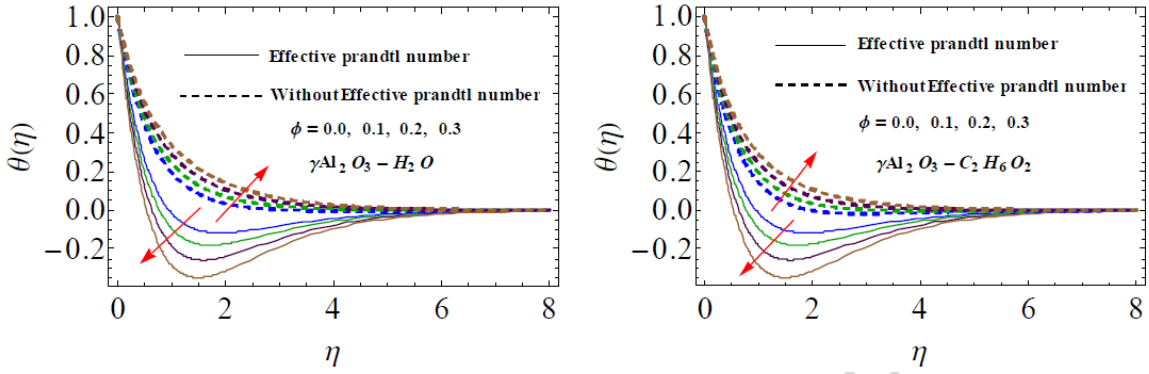

Figure 3

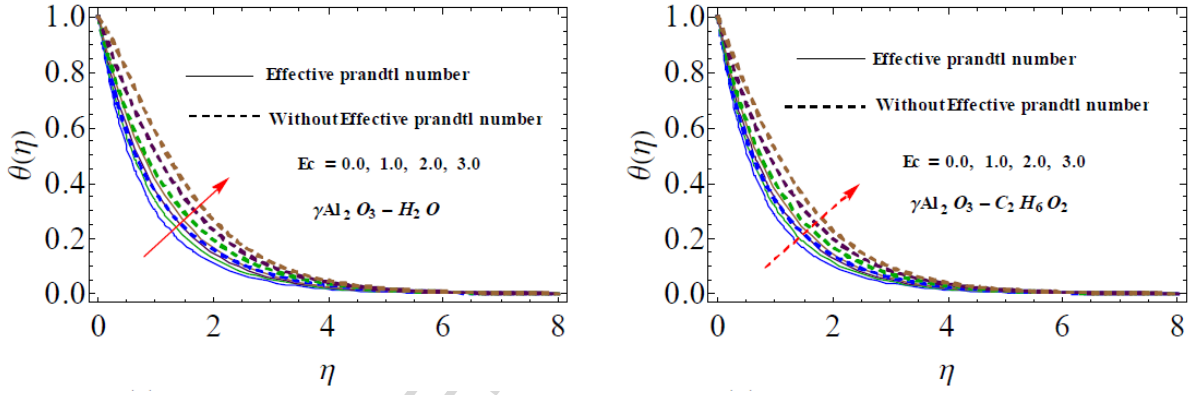

Figure 4

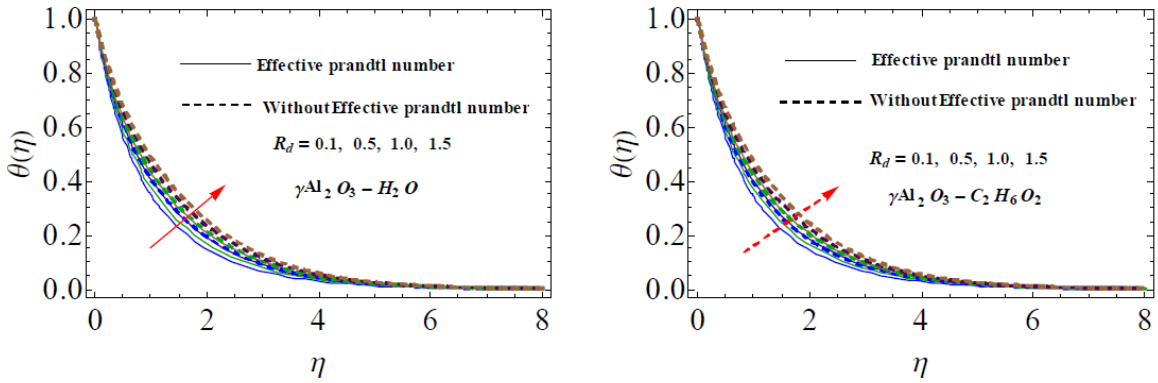

Figure 5

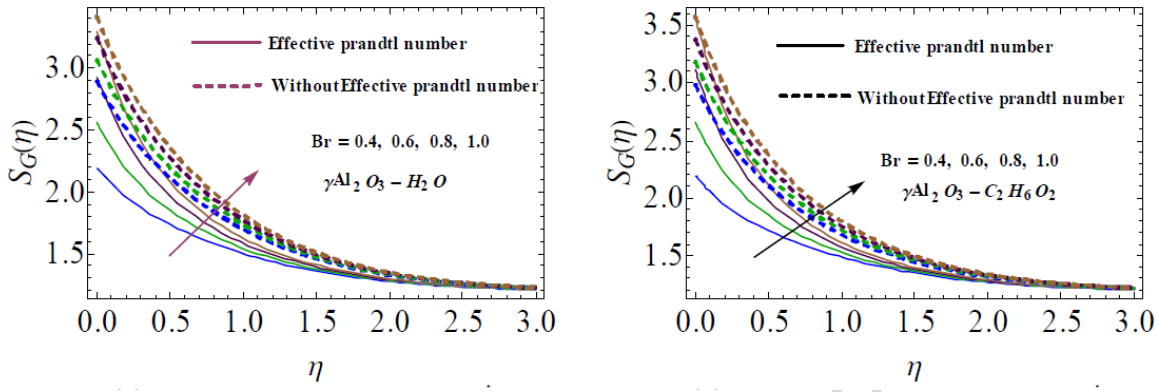

Figure 6

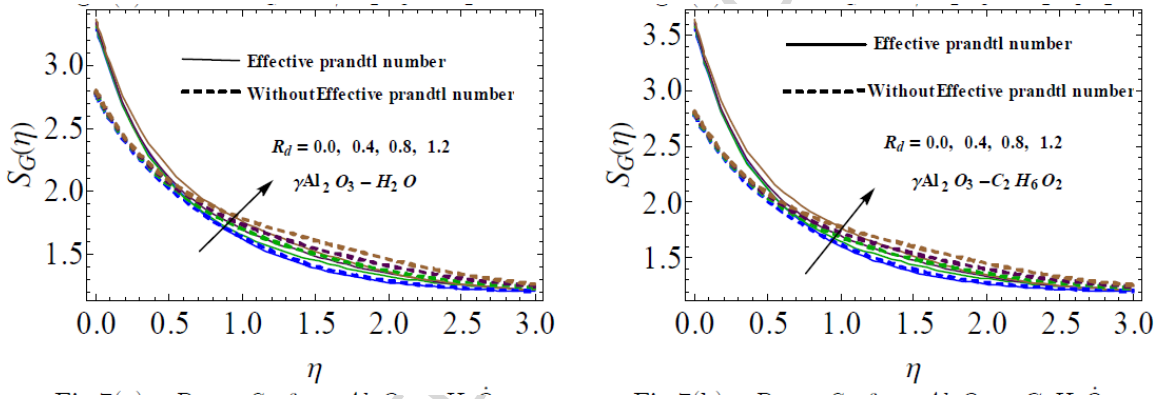

Figure 7

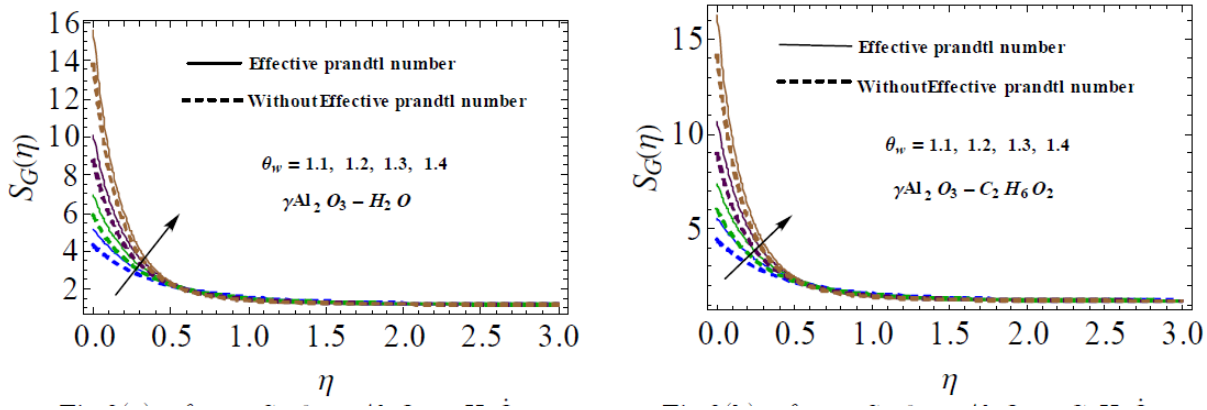

Figure 8

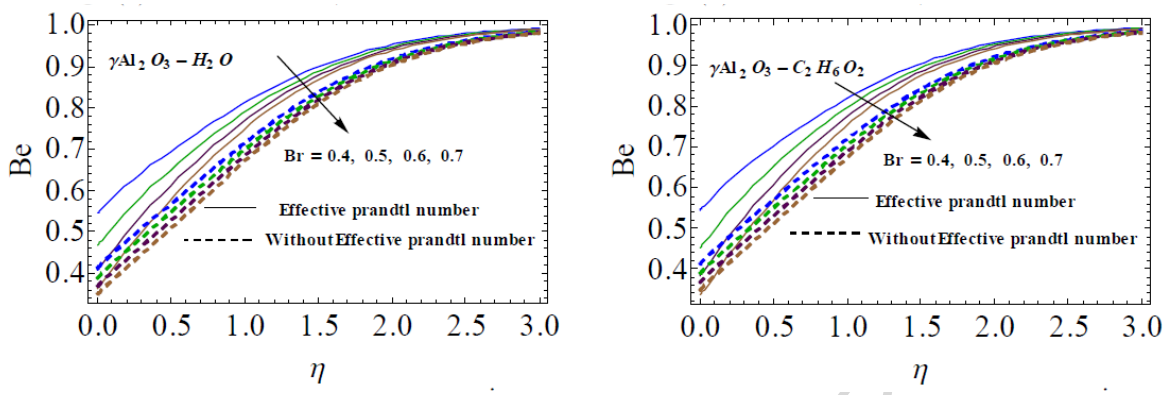

Figure 9

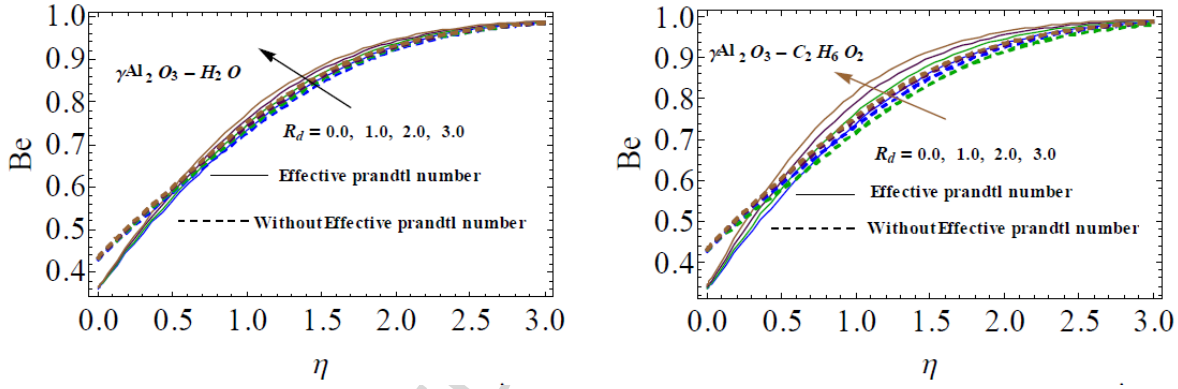

Figure 10

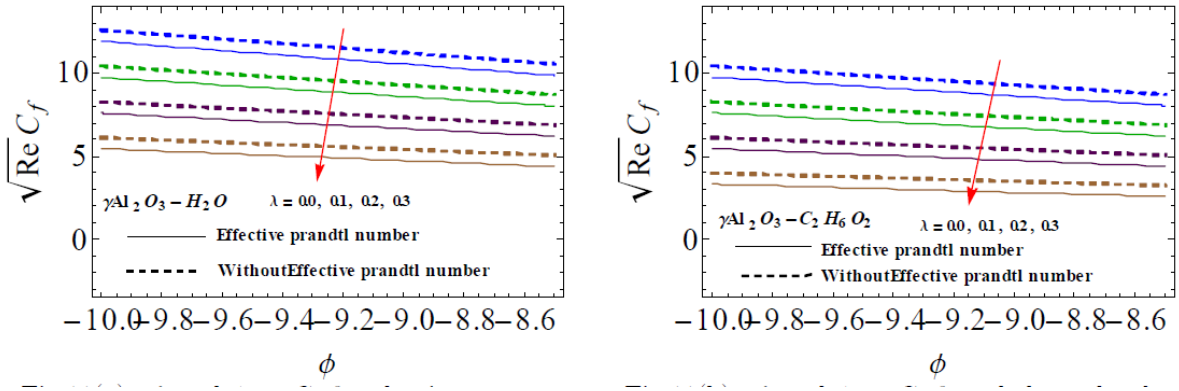

Figure 11

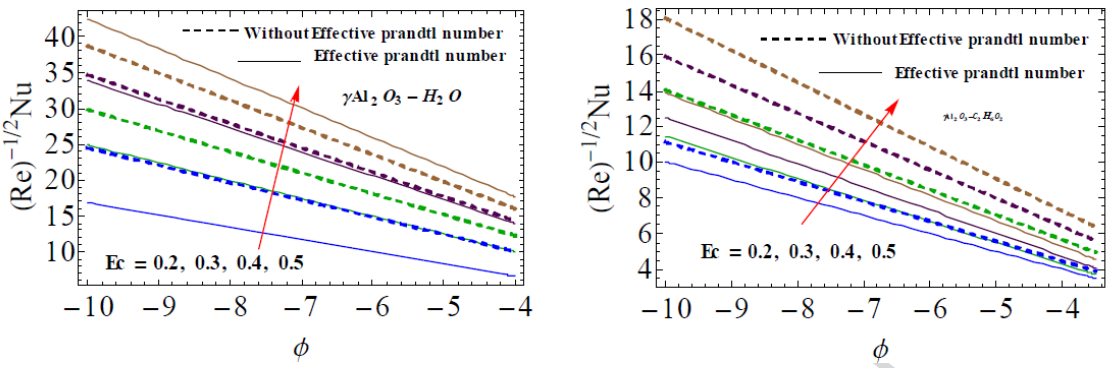

Figure 12

Highlights

- Entropy generation optimization regarding nonlinear radiative heat flux is discussed.
- Thermodynamic second law is implemented in modeling.
- Nanoparticles comprise (γAl_2O_3-H_2O and γAl_2O_3-$C_2H_6O_2$) particles.
- A optimal homotopy technique is implemented for the solutions development.
- Optimal values of auxiliary parameters are calculated.

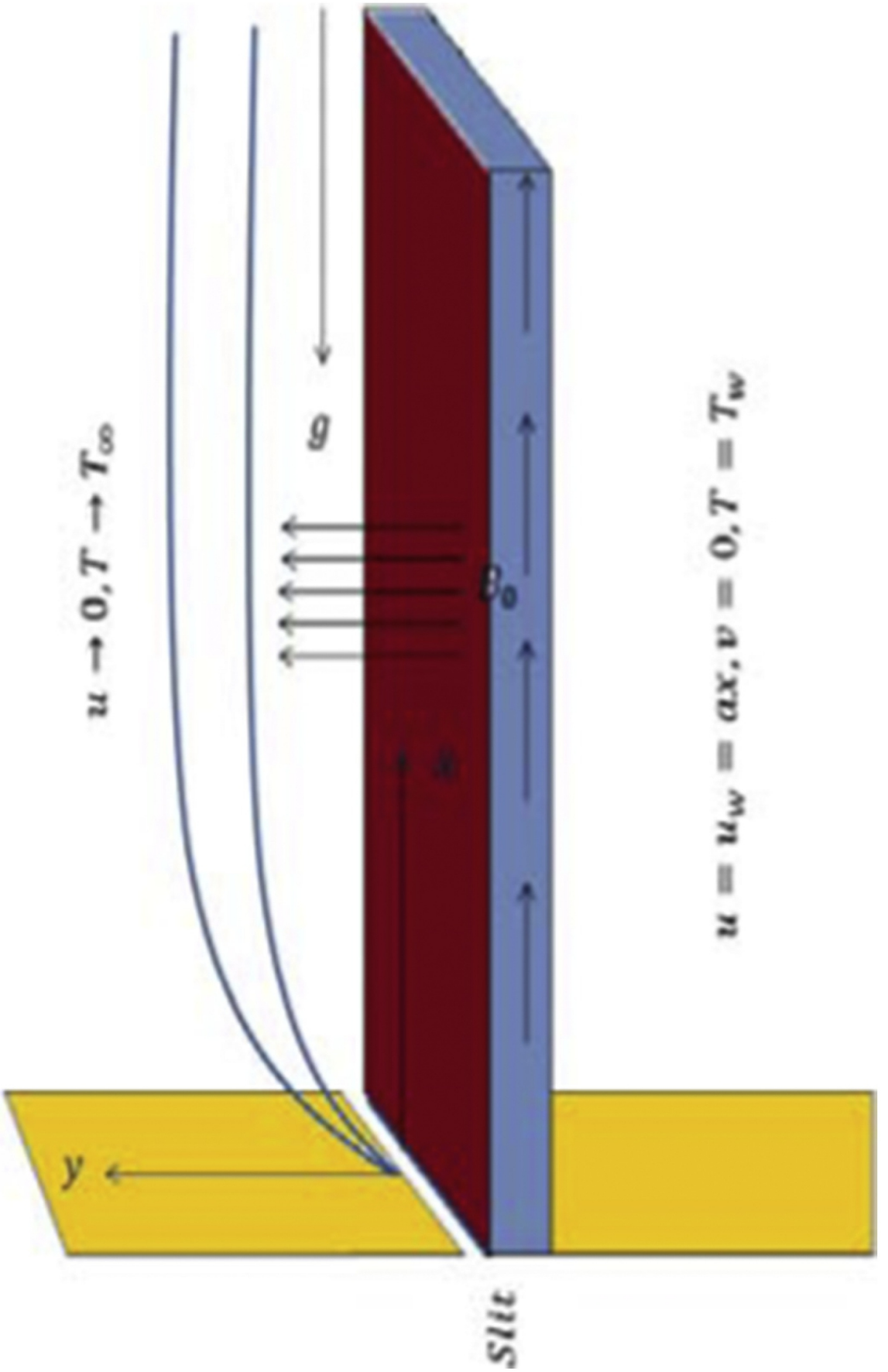

Figure 1

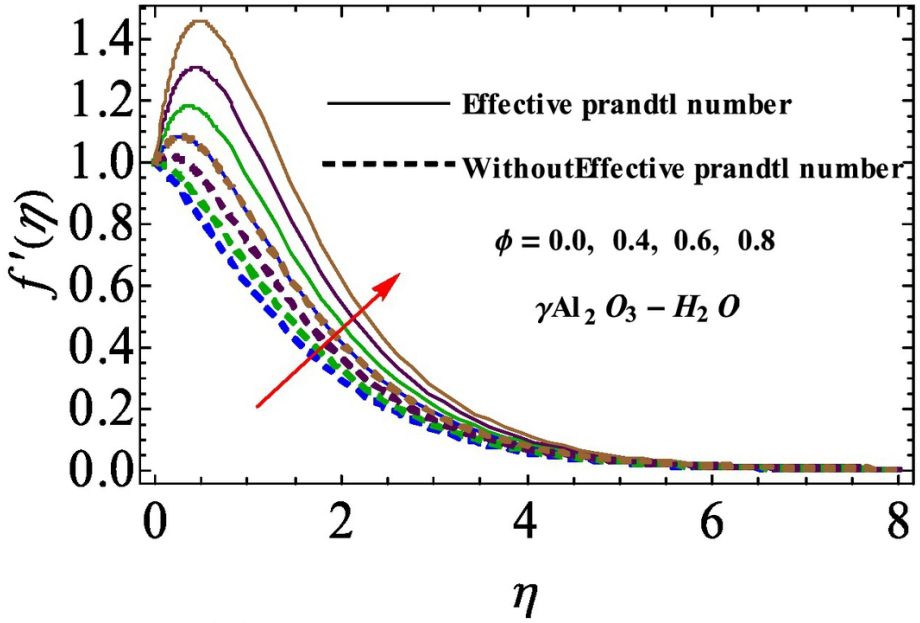

(a) : ϕ on f' for $\gamma Al_2O_3 - H_2O$.

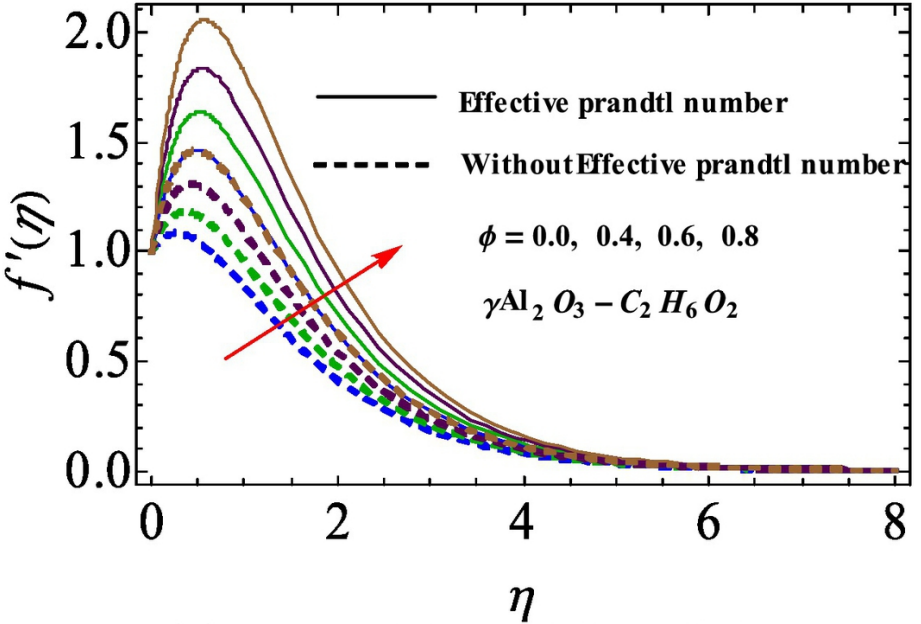

(b) : ϕ on f' for $\gamma Al_2O_3 - C_2H_6O_2$.

Figure 2

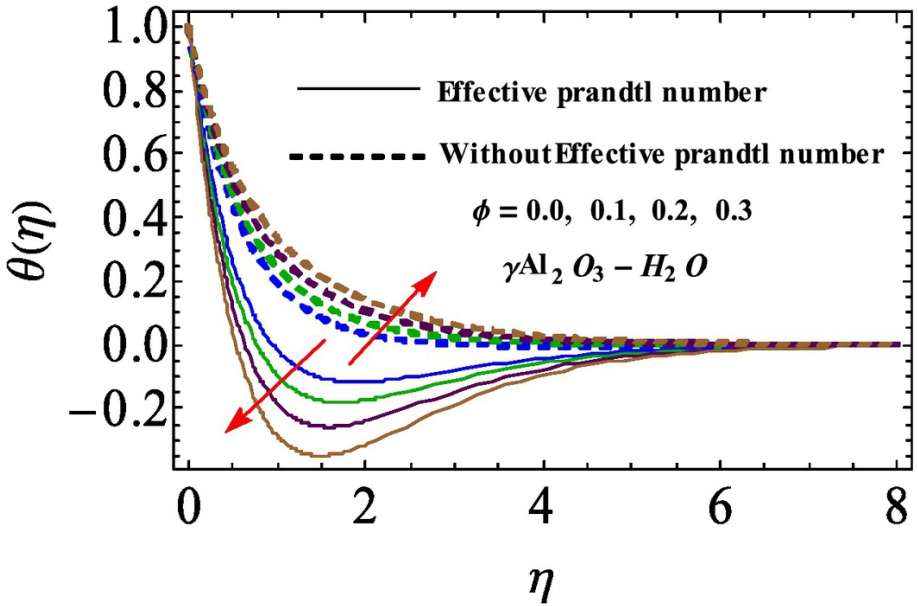

(a) : ϕ on θ for $\gamma Al_2O_3 - H_2O$.

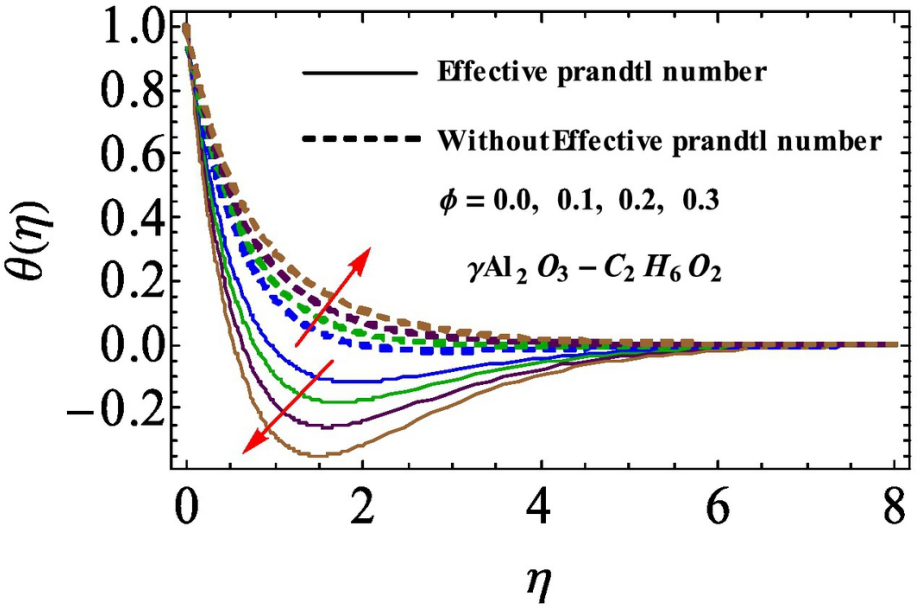

(b) : ϕ on θ for $\gamma Al_2O_3 - C_2H_6O_2$.

Figure 3

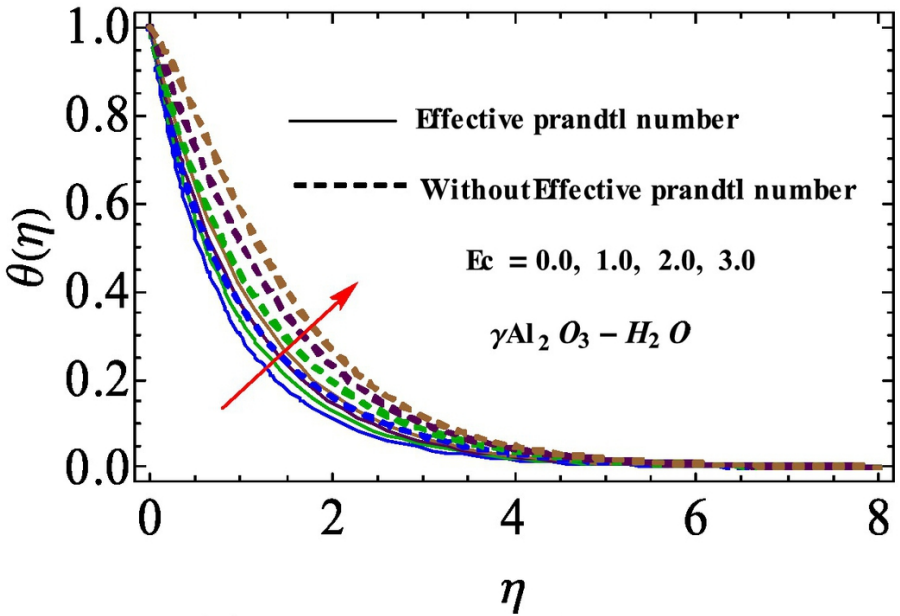

(a) : Ec on θ for $\gamma Al_2O_3 - H_2O$.

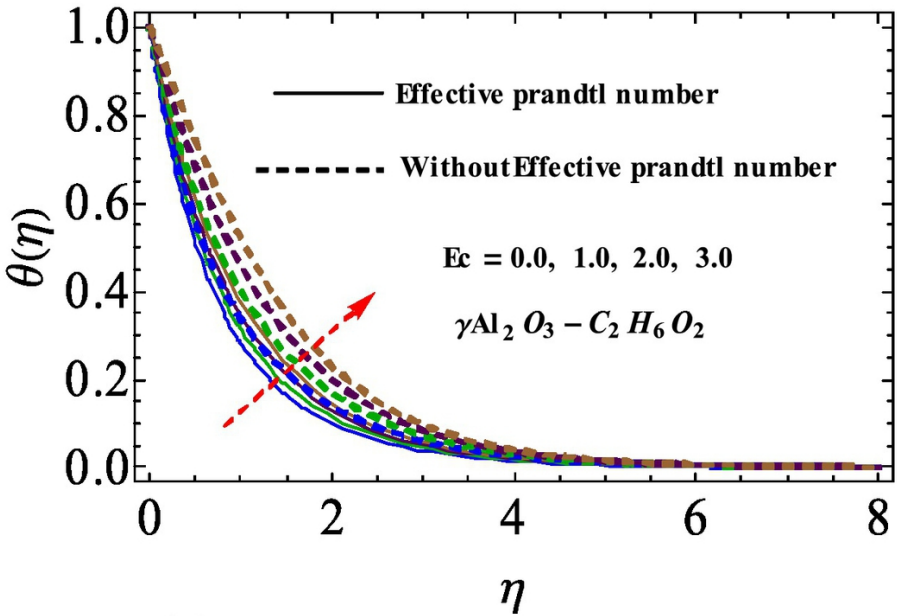

(b) : Ec on θ for $\gamma Al_2O_3 - C_2H_6O_2$.

Figure 4

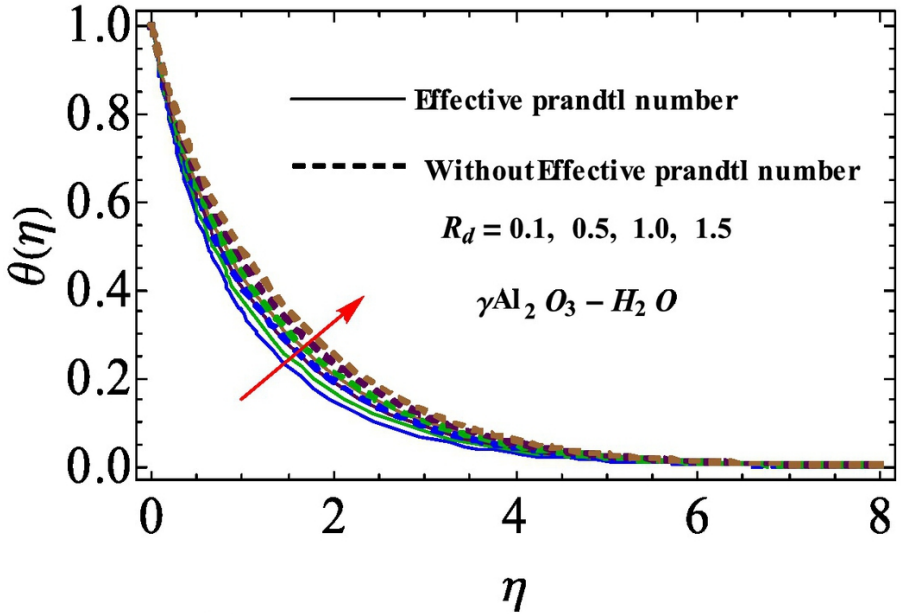

(a) : R_d on θ for $\gamma Al_2O_3 - H_2O$.

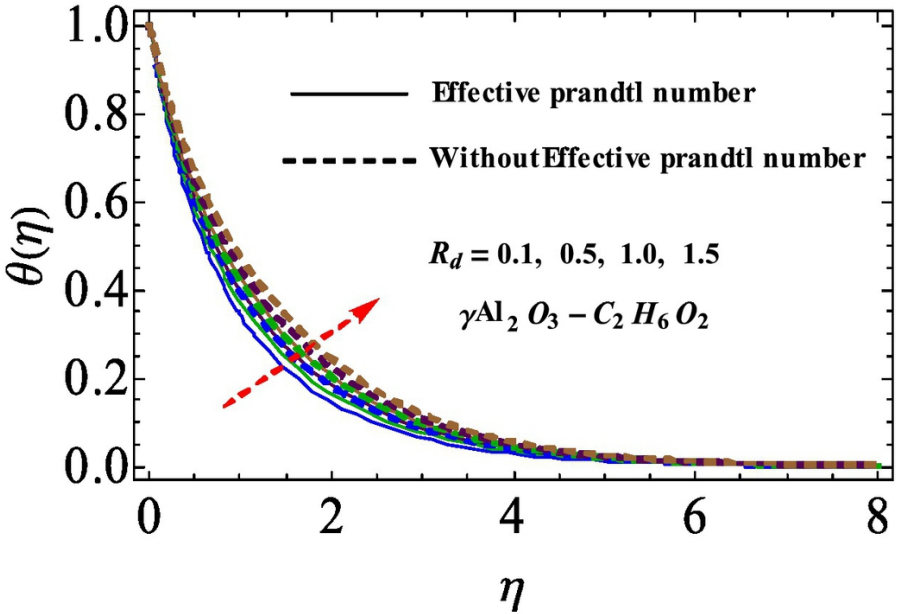

(b) : R_d on θ for $\gamma Al_2O_3 - C_2H_6O_2$.

Figure 5

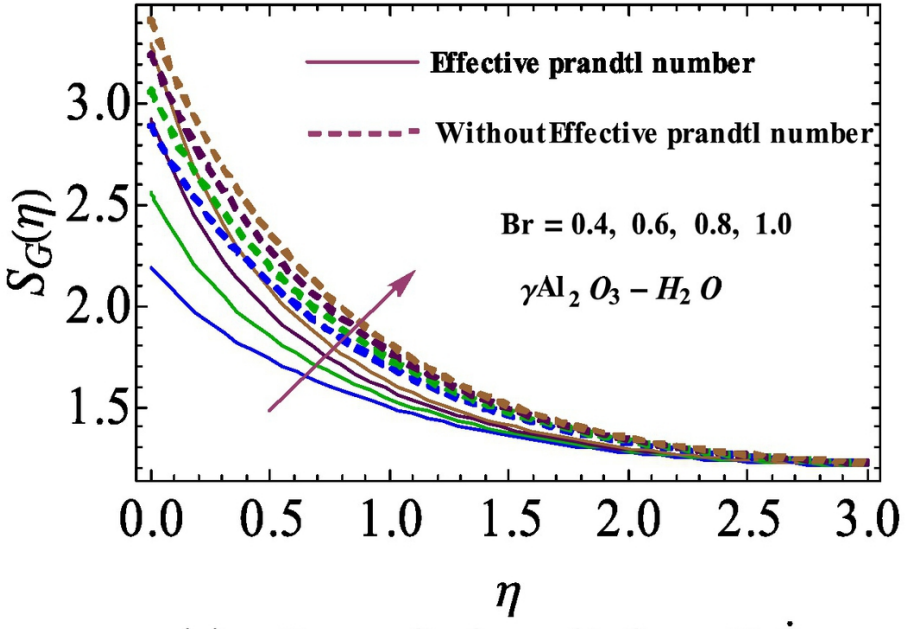

(a) : Br on S_G for $\gamma Al_2O_3 - H_2\dot{O}$.

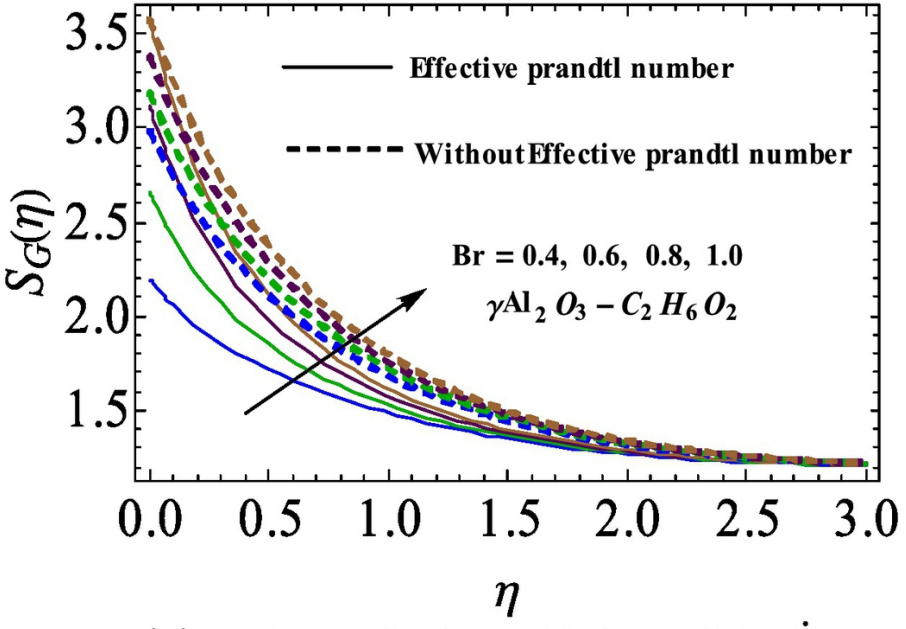

(b) : Br on S_G for $\gamma Al_2O_3 - C_2H_6\dot{O}_2$.

Figure 6

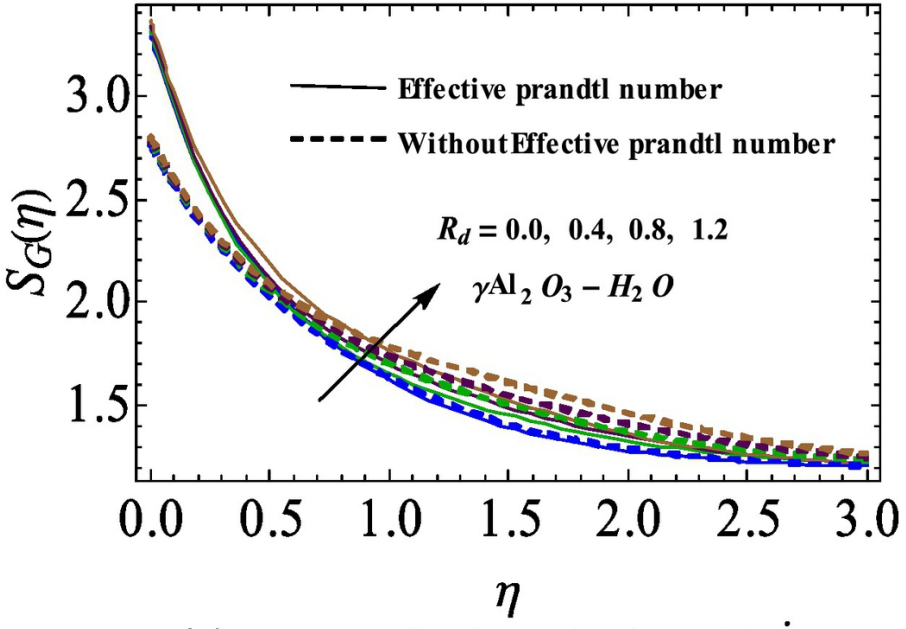

(a) : R_d on S_G for $\gamma Al_2O_3 - H_2\dot{O}$.

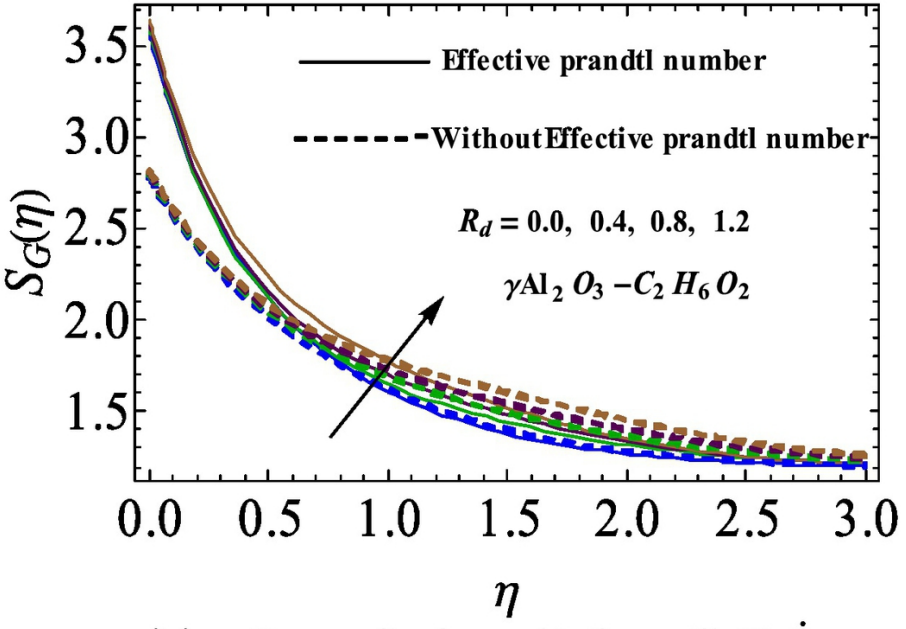

(b) : R_d on S_G for $\gamma Al_2O_3 - C_2H_6\dot{O}_2$.

Figure 7

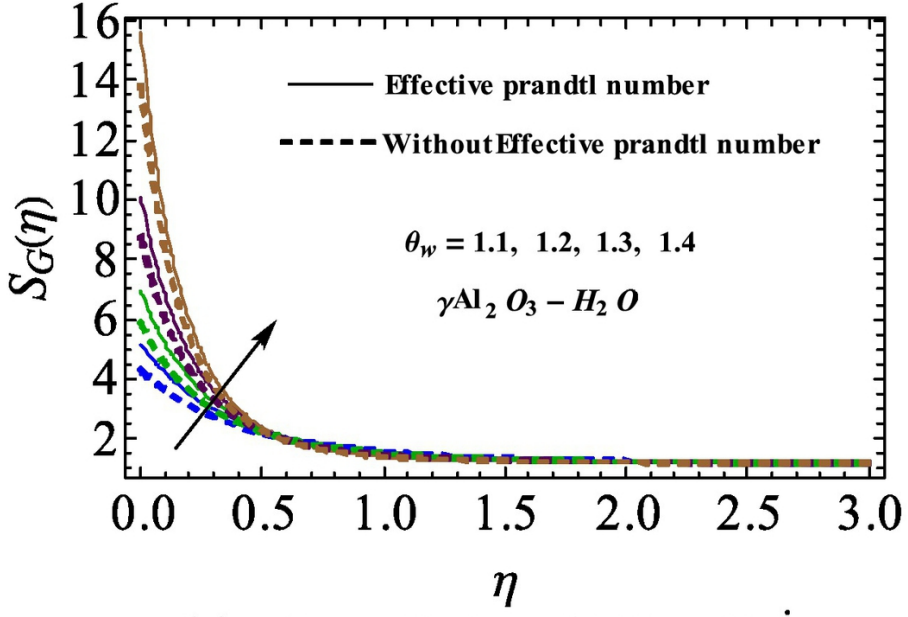

(a) : θ_w on S_G for $\gamma Al_2O_3 - H_2\dot{O}$.

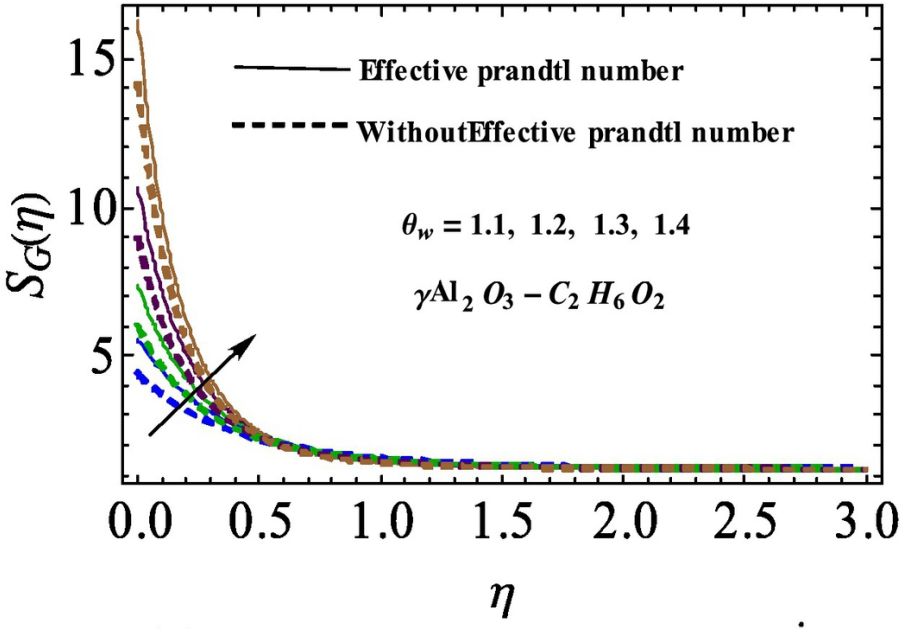

(b) : θ_w on S_G for $\gamma Al_2O_3 - C_2H_6\dot{O}_2$.

Figure 8

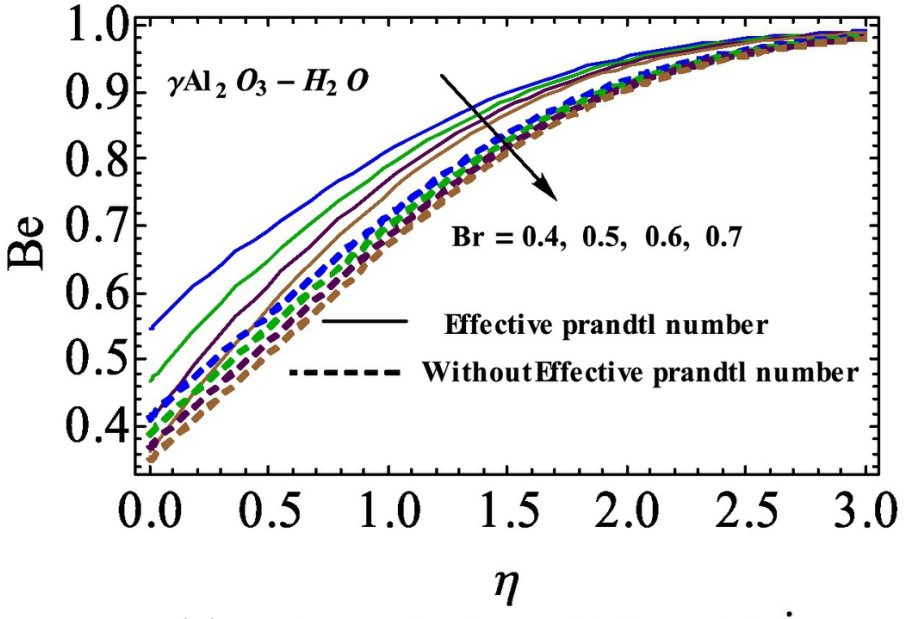

(a) : Br on Be for $\gamma Al_2O_3 - H_2\dot{O}$.

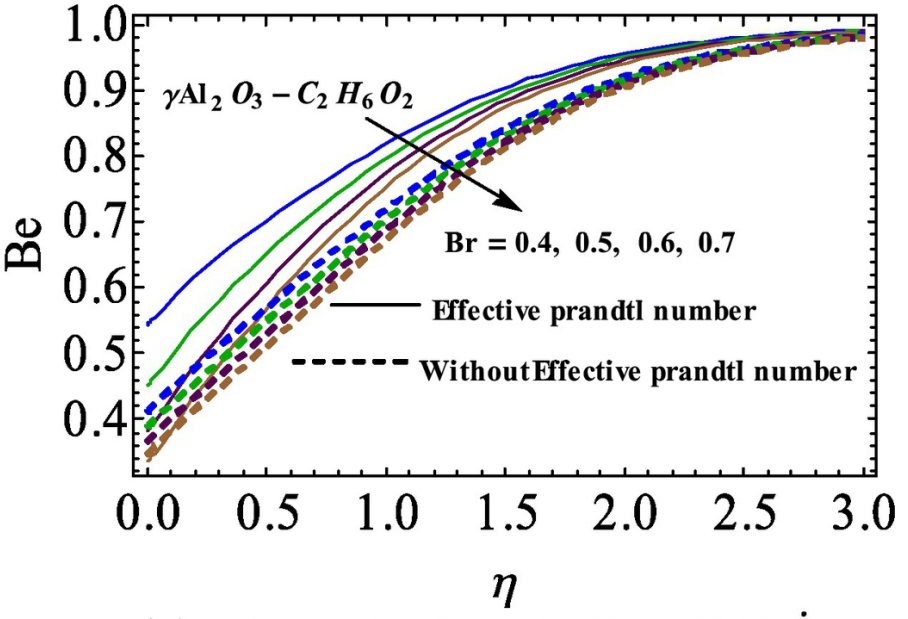

(b) : Br on Be for $\gamma Al_2O_3 - C_2H_6\dot{O}_2$.

Figure 9

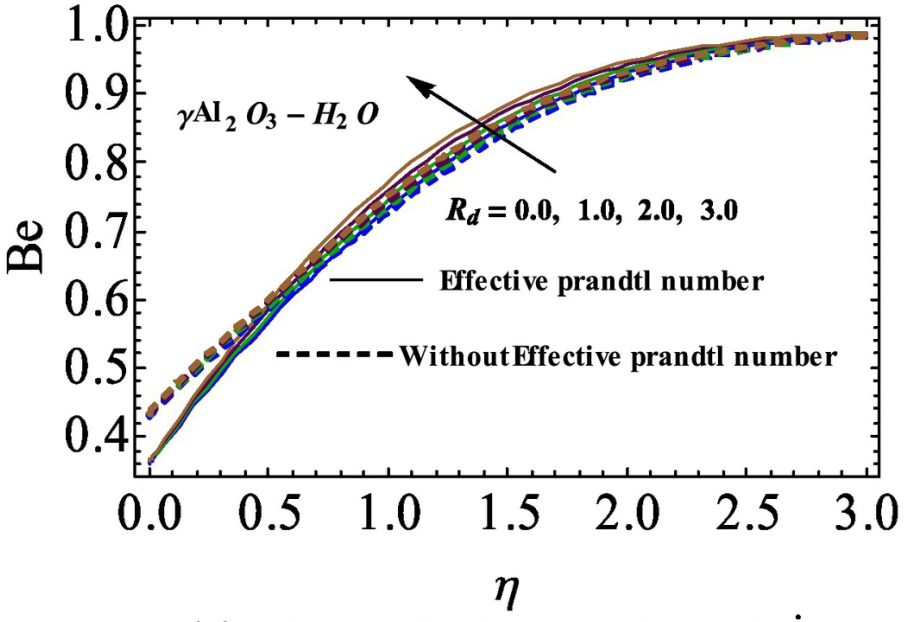

(a) : R_d on Be for $\gamma Al_2O_3 - H_2\dot{O}$.

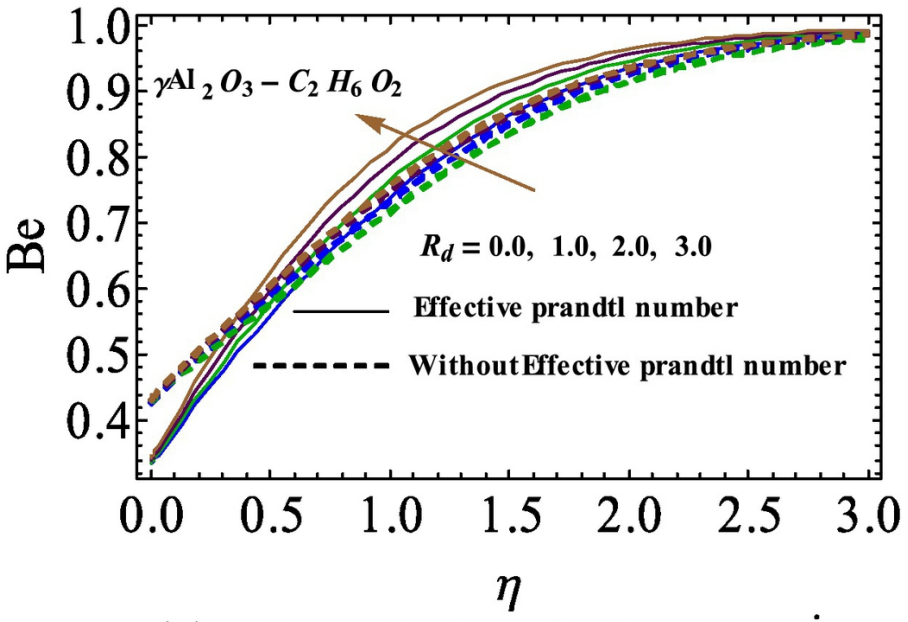

(b) : R_d on Be for $\gamma Al_2O_3 - C_2H_6\dot{O}_2$.

Figure 10

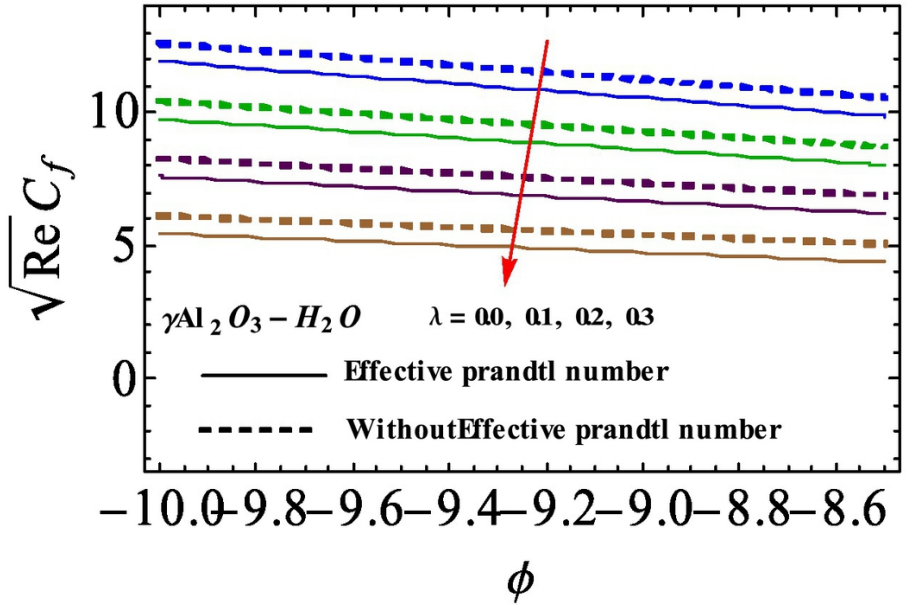

(a) : λ and ϕ on C_f for alumina water.

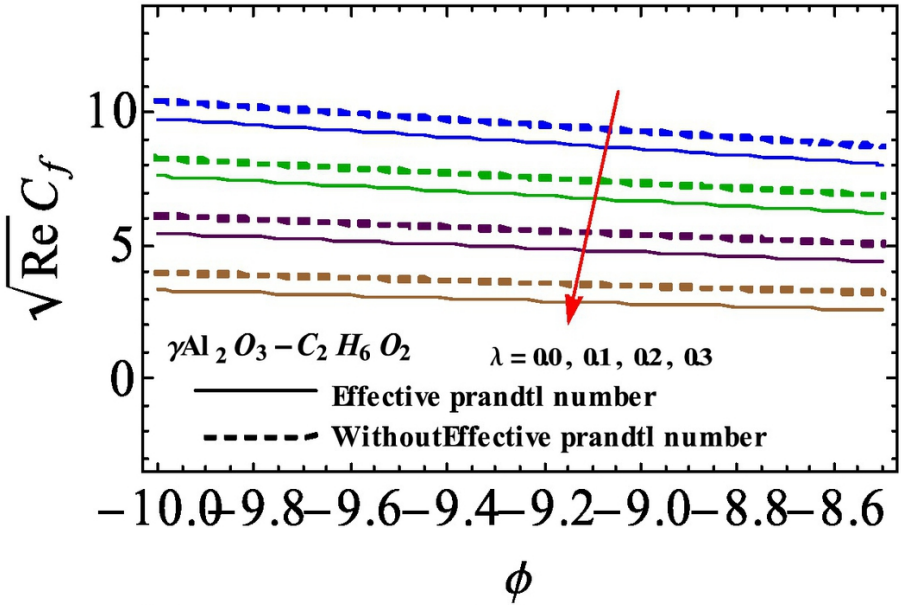

(b) : λ and ϕ on C_f for ethylenecglycol.

Figure 11

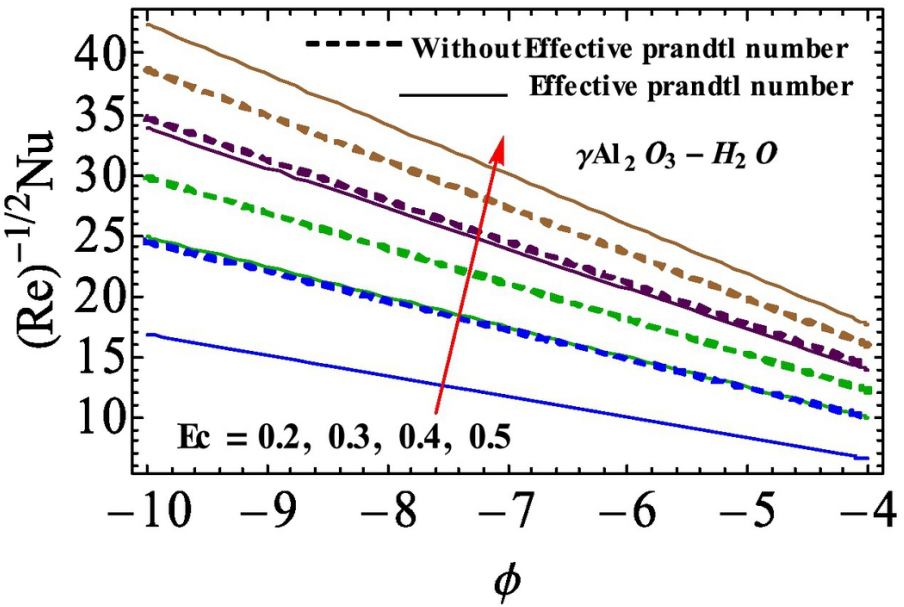

(a) : Ec and ϕ on Nu for alumina water.

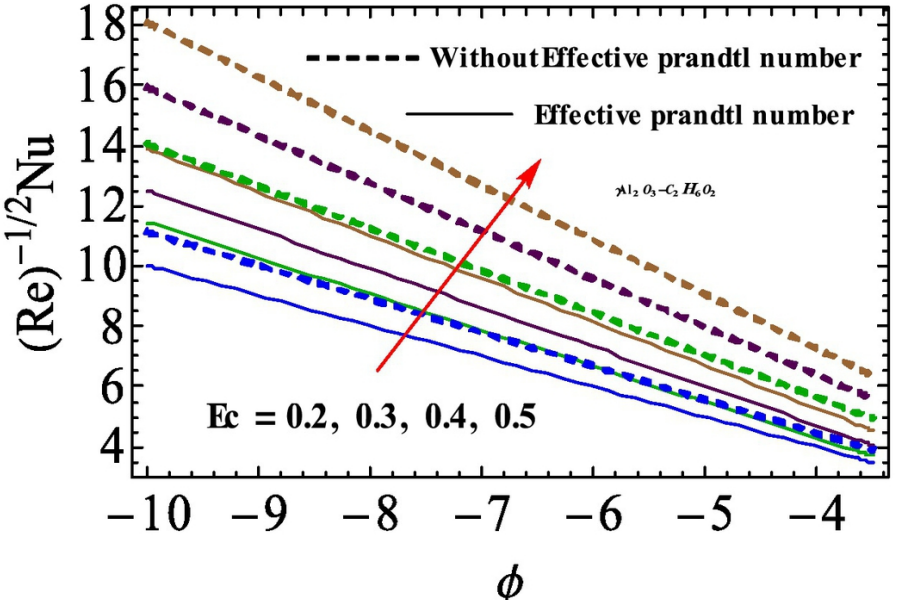

(b) : Ec and ϕ on Nu for ethylenecglycol .

Figure 12